Y. Shi, S. Wang, K. Wang, R. Yang, D. Liu, H. Liao, Y. Qi, K. Qiu, Y. Hu, H. Wen,* K. Xu*

Relieving Macrophage Dysfunction by Inhibiting SREBP2 Activity: A Hypoxic Mesenchymal Stem Cells-Derived Exosomes Loaded Multifunctional Hydrogel for Accelerated Diabetic Wound Healing

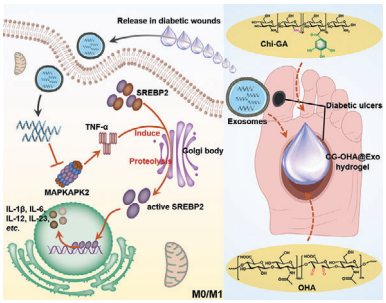

A multifunctional hydrogel consisting of gallic acid (GA) conjugated chitosan (Chi-GA) and partially oxidized hyaluronic acid (OHA) is prepared as a vehicle of hypoxic mesenchymal stem cells-derived exosomes to relieve macrophage dysfunction during diabetic wound healing. The underlying molecular mechanism may be that exosomal miR-4645-5p and antioxidant property of the hydrogel synergistically inhibit SREBP2 activity in macrophages.

NANO · MICRO small
www.small-journal.com

Relieving Macrophage Dysfunction by Inhibiting SREBP2 Activity: A Hypoxic Mesenchymal Stem Cells-Derived Exosomes Loaded Multifunctional Hydrogel for Accelerated Diabetic Wound Healing

Yan Shi, Shang Wang, Kai Wang, Ronghua Yang, Dewu Liu, Huaiwei Liao, Yuhan Qi, Keqing Qiu, Yanghong Hu, Huicai Wen, and Kui Xu**

Macrophage dysfunction is one of the primary factors leading to the delayed healing of diabetic wounds. Hypoxic bone marrow mesenchymal stem cells-derived exosomes (hyBMSC-Exos) have been shown to play an active role in regulating cellular function through the carried microRNAs. However, the administration of hyBMSC-Exos alone in diabetic wounds usually brings little effect, because the exosomes are inherently unstable and have a short retention time at the wounds. In this study, a multifunctional hydrogel based on gallic acid (GA) conjugated chitosan (Chi-GA) and partially oxidized hyaluronic acid (OHA) is prepared for sustained release of hyBMSC-Exos. The hydrogel not only exhibits needs-satisfying physicochemical properties, but also displays outstanding biological performances such as low hemolysis rate, strong antibacterial capacity, great antioxidant ability, and excellent biocompatibility. It has the ability to boost the stability of hyBMSC-Exos, leading to a continuous and gradual release of the exosomes at wound locations, ultimately enhancing the exosomes' uptake efficiency by target cells. Most importantly, hyBMSC-Exos loaded hydrogel shows an excellent ability to promote diabetic wound healing by regulating macrophage polarization toward M2 phenotype. This may be because exosomal miR-4645-5p and antioxidant property of the hydrogel synergistically inhibit SREBP2 activity in macrophages. This study presents a productive approach for managing diabetic wounds.

1. Introduction

Diabetic foot ulcer (DFU) is a prevalent, serious and costly complication of diabetic mellitus (DM), and has emerged as a major challenge for healthcare systems worldwide.[1] It is estimated that ≈15–19% of individuals diagnosed with DM will encounter DFU during their lifetime.[2] DFU often puts patients at great risk of infection, amputation, and even premature death. The 5-year mortality rate and direct care costs of DFU are almost comparable to those of all-cause cancer, and over 85% of non-traumatic lower limb amputations are preceded by foot ulcers.[3] Traditional clinical treatments for DFU mainly focus on surgical debridement, skin grafting, and negative pressure therapy, but the treatment effect is usually not satisfactory.[4] These facts strongly imply the need of more effective and easily applicable therapeutic strategies for DFU management.

Impaired wound healing represents the leading cause of DFU, which is characterized by continuous inflammation,

Y. Shi, H. Liao, Y. Qi, H. Wen
Department of Plastic
Medical Center of Burn Plastic and Wound Repair
The First Affiliated Hospital
Jiangxi Medical College
Nanchang University
Nanchang, Jiangxi 330006, P. R. China
E-mail: 13907082146@163.com

S. Wang
Chongqing Key Laboratory of Traditional Chinese Medicine for Prevention and Cure of Metabolic Diseases
College of Traditional Chinese Medicine
Chongqing Medical University
Chongqing 400016, P. R. China

The ORCID identification number(s) for the author(s) of this article can be found under https://doi.org/10.1002/smll.202309276

K. Wang, K. Xu
Key Laboratory of Xin'an Medicine
Ministry of Education
Anhui University of Chinese Medicine
Hefei, Anhui 230038, P. R. China
E-mail: kueikui.hsu@gmail.com

R. Yang
Department of Burn and Plastic Surgery
Guangzhou First People's Hospital
South China University of Technology
Guangzhou, Guangdong 510650, P. R. China

D. Liu
Medical Center of Burn Plastic and Wound Repair
The First Affiliated Hospital of Nanchang University
Nanchang, Jiangxi 330006, P. R. China

DOI: 10.1002/smll.202309276

inhibited angiogenesis, and disturbed fibroblasts maturation.[5] This is most likely due to dysregulated macrophage phenotype switch.[5] During a normal wound healing, macrophages can naturally undergo a specific inflammatory-to-reparative phenotype (M1-to-M2) switch for establishing the healing cascade.[6] The activation of M2 triggers the production of various types of cytokines, including interleukin (IL)−10, insulin-like growth factor (IGF), transforming growth factor (TGF)-β1, vascular endothelial growth factor (VEGF), and others, which leads to accelerated angiogenesis, re-epithelialization, and proper collagen remodeling.[7] In diabetic wounds, however, there is a failure to maintain the equilibrium of macrophage polarization, resulting in an excessive accumulation of M1 macrophages. The cells continuously express pro-inflammatory cytokines (e.g., IL-1β, IL-6, IL-12, IL-23, tumor necrosis factor-α (TNF-α)) at high levels.[8] In addition to promoting the inflammatory response in the wounds, the cytokines also hinder the formation of new blood vessels and impair the proliferation of keratinocytes, thus slowing down the remodeling of new wound tissues.[9] Therefore, how to relieve the dysfunction of macrophages that are unable to polarize towards M2 phenotype is one of the key challenges that must be solved to explore novel and effective therapeutic strategies for DFU.

Fortunately, exosomes from stem cells offer more possibilities for the regulation of macrophage function. This is because they can transport a variety of microRNAs, specific proteins, lipids, and glycoconjugates, thereby influencing intercellular communication and various cellular processes.[10] Due to the immunomodulatory and anti-inflammatory performances of mesenchymal stem cells (MSCs), MSCs-derived exosomes (MSC-Exos) have attracted more and more attention in recent years.[11] A study of Ren et al. proved that MSC-Exos can promote macrophage M2 polarization by increasing miR-21-5p delivery.[12] Cao et al. observed that exosomal microRNAs derived from adipose mesenchymal stem cells improved polycystic ovary syndrome by preventing metabolic disorders.[13] As one of the most common and readily available stem cells, bone marrow mesenchymal stem cells (BMSCs) are situated in an environment with restricted oxygen availability (ranging from 1% to 6%).[14] Hypoxic microenvironment may boost BMSCs' multipotentiality and proliferation, and can favor in vitro expansion culture of BMSCs.[15] Our previous studies suggest that hypoxia treatment can intensify BMSCs' paracrine ability and enhance the production of exosomes and exosomal factor species.[16] Moreover, hypoxic BMSCs (hyBMSCs)-derived exosomes (hyBMSC-Exos) has shown a promising application prospect in the field of bone regeneration.[17] However, the administration of hyBMSC-Exos for regulating dysfunctional macrophages in the complex diabetic microenvironments still faces serious challenges. One the one hand, it is urgent to seek a satisfactory carrier for the exosomes. They are mainly administered by injection, which undeniably reduces their therapeutic effectiveness as a result of rapid clearance.[18] Furthermore, it is difficult to achieve sustained release of hyBMSC-Exos by local injection to maintain their bioactivity throughout the duration of diabetic wound healing. Also, the exosomes do not possess antibacterial and antioxidative properties as well as appropriate physicochemical properties necessary for diabetic wound dressings. One the other hand, the underlying mechanism of hyBMSC-Exos regulating macrophage dysfunction in diabetic wounds is poorly explored and thus remains unclear. Studies have shown that one of the main means of hyBMSC-Exos treating diseases is to regulate cell signaling pathways via releasing the carried microRNAs.[19] The findings of our previous study have demonstrated that miR-4546-5p derived from hyBMSC-Exos may be efficacious in treatment of impeded transition from the inflammatory phase to the resolution stage during wound healing progression.[16b] So does this imply that miR-4546-5p may plays a crucial role in macrophage polarization towards M2 phenotype regulated by hyBMSC-Exos?

To address the problems, it would be desirable that an application of a multifunctional exosomes-loaded formulation, such as a hydrogel, can steadily and persistently deliver exosomes to promote diabetic wound healing. Many studies have fully demonstrated that hydrogels as exosome carriers can achieve the unique effect of killing three birds with one stone, namely maintaining the structural integrity of exosomes, in situ sustained release of exosomes, and performance plasticity.[20] In this work, therefore, a multifunctional hydrogel consisting of gallic acid (GA) conjugated chitosan (Chi-GA) and partially oxidized hyaluronic acid (OHA) was prepared as a vehicle of hyBMSC-Exos to relieve macrophage dysfunction during diabetic wound healing (**Figure 1**). Extracted from various plants and fruits, GA is a natural plant polyphenol that exhibits excellent biocompatibility, nontoxicity, and non-immunogenicity.[21] Of greater significance, GA possesses exceptional antioxidant property and strong adhesion to the wounds due to the presence of three phenolic hydroxyl groups.[21,22] And owing to the introduction of phenolic hydroxyl and aldehyde groups in the hydrogel, hyBMSC-Exos can be anchored into the carrier by Schiff base and Markell addition reactions (Figure 1).[23] It is expected that this can not only maintain the stability of the exosomes, but also achieve in situ sustained release of the exosomes at wound sites.

All in all, we may hypothesize that hyBMSC-Exos loaded multifunctional hydrogel has the potential to greatly accelerate diabetic wound healing due to its favorable biocompatibility, antioxidative and antibacterial properties, and its capability to regulate macrophage polarization. And the underlying mechanism of hyBMSC-Exos regulating macrophage polarization towards M2 phenotype may involve signaling pathways that are closely related to miR-4546-5p. In order to confirm the hypotheses as accurately as possible, physicochemical properties of the hydrogel will be evaluated, subsequently examining in vitro biological effects related to diabetic wound healing, particularly focusing on the influence and mechanism of the hydrogel on macrophage polarization. Following this, we will employ a mouse diabetic wound model to assess the

K. Qiu
Dermatological Department
The Second Affiliated Hospital of Nanchang University
Nanchang, Jiangxi 330006, P. R. China
Y. Hu
Jiangxi University of Chinese Medicine
Nanchang, Jiangxi 330006, P. R. China

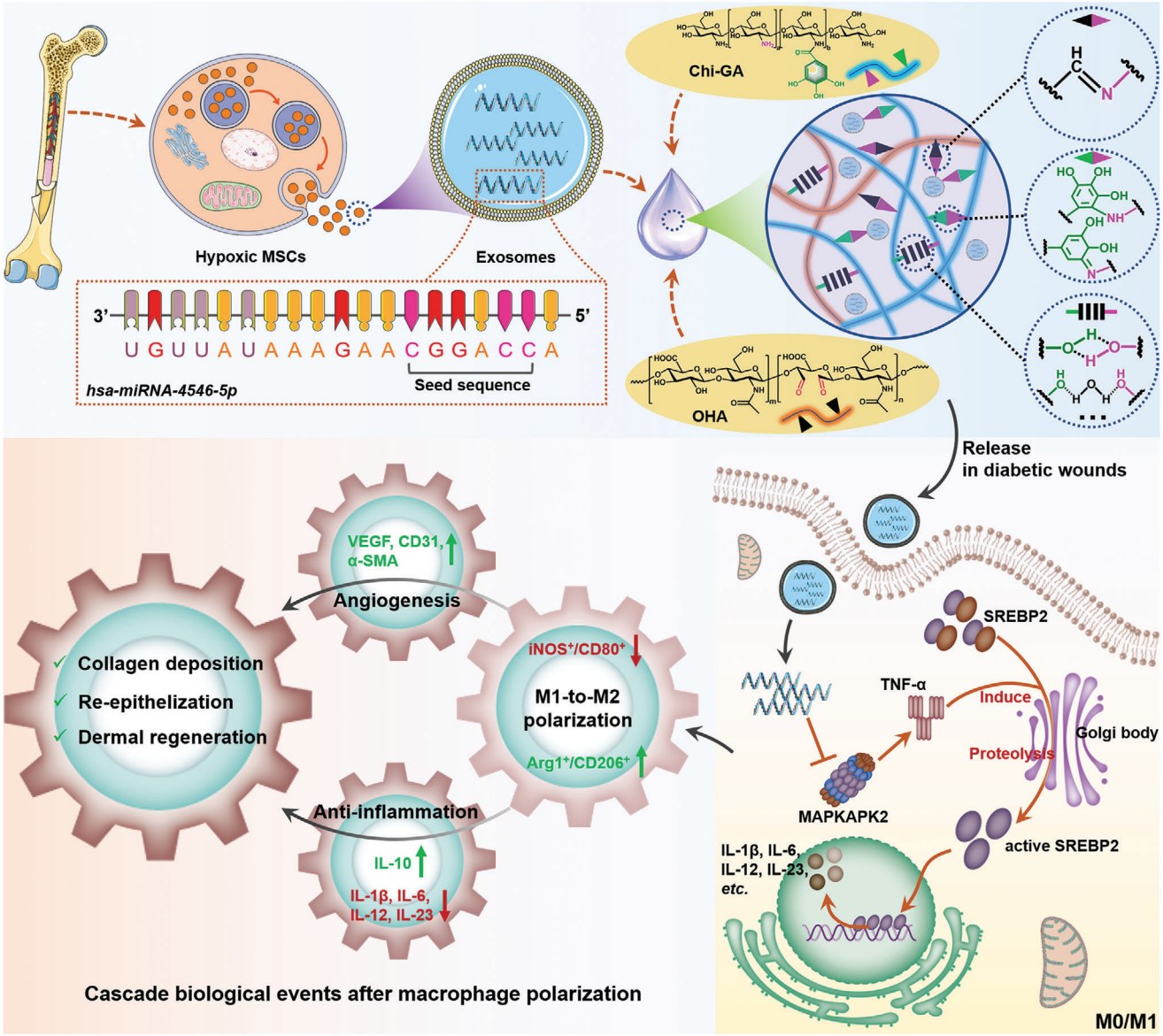

Figure 1. A schematic diagram for illustrating CG-OHA@Exo hydrogel preparation and the underlying mechanism of it accelerating diabetic wound healing.

efficacy of the hydrogel in enhancing diabetic wound healing in vivo.

2. Results and Discussion

2.1. Preparation and Characterization of hyBMSC-Exos

Hypoxia-induced factor-1 alpha (HIF-1α) is commonly present in human and mammalian cells, and is also expressed in the presence of typical oxygen levels (21% O_2). However, the produced HIF-1α undergoes swift degradation through the intracellular oxygen-dependent ubiquitin-protease degradation pathway, and thus HIF-1α can be stably expressed only under a hypoxic condition.[24] Hypoxia treatment has no significant effect on the morphology of BMSCs (Figure S1a, Supporting Information). Figure S1b (Supporting Information) displays representative immunofluorescence images indicating significant accumulation of HIF-1α in BMSCs subjected to hypoxia (1% O_2) for 48 h. Despite being widely recognized as the most commonly used and dependable technique for exosome isolation, ultracentrifugation has limitations in terms of yield and purity.[25] In this study, therefore, we implemented a protocol for exosome extraction and refinement via following the comprehensive instructions provided by the International Society for Extracellular Vesicles,[26] which is outlined in Figure S1c (Supporting Information). Low-speed centrifugation and size exclusion were performed prior to ultracentrifugation to enable exclusion of cells, debris, large apoptotic bodies, and micro-vesicles. The results of field emission transmission electron microscopy (FE-TEM) confirm the isolated vesicles to have round-shaped exosome morphology with

the bounded membrane (Figure S1d, Supporting Information). According to the nanoparticle tracking analysis, the vast majority of the isolated vesicles are found to be in the range of 50 to 150 nanometers in diameter, with a peak at 141 nm (Figure S1e, Supporting Information). This finding aligns with the previously reported size of exosomes.[27] Further, western blotting analysis of CD9, CD63, and CD81 was carried out to identify hyBMSC-Exos.[28] As shown in Figure S1f (Supporting Information) and Figure S2 (Supporting Information), the isolated vesicles are positive for those three kinds of exosomal surface proteins. Interestingly, hypoxia treatment induces the higher expression of CD63 in BMSCs, indicating that more exosomes are produced inside the cells. Meanwhile, bicinchoninic acid (BCA) protein assay reveals that ≈1 μg of exosomal proteins could be extracted per million hyBMSCs, surpassing previously reported results.[29] The aforementioned findings suggest that hyBMSC-Exos are successfully and efficiently extracted by the above standard exosome isolation and purification procedure.

2.2. Preparation and Characterization of Hydrogels

The synthesis of Chi-GA involves a coupling reaction between amino and carboxyl groups catalyzed by N-(3-dimethylaminopropyl)-N'-ethylcarbodiimide (EDC)/N-hydroxysuccinimide (NHS), leading to the grafting of GA to the backbone of Chi (Figure S3a, Supporting Information). As displayed in Figure S3b (Supporting Information), a specific peak at 6.988 ppm should be assigned to aromatic ring proton on GA molecular.[30] Figure S3c (Supporting Information) shows the FTIR spectra of Chi and Chi-GA. C = O stretching vibration in the N-acetyl group at 1634 cm^{-1} is greatly intensified duo to the reaction between the primary amine of Chi and the carboxyl group of GA,[30b,31] while N-H deformation vibration in primary amine at 1593 cm^{-1} experiences a significant reduction.[22b,32] More importantly, a new peak appeared at 1544 cm^{-1} is C = C stretching vibration peak of aromatic ring,[30b,33] forcefully indicating that GA has been introduced into Chi backbone. Furthermore, the ultraviolet-visible (UV–vis) spectra of Chi and Chi-GA samples were investigated in view of the aromatic ring structure in the GA molecule, and the results are illustrated in Figure S3d (Supporting Information). A new peak with weak intensity at ≈275 nm appears in the spectrum of Chi-GA owing to the presence of benzene ring.[22b] These results strongly prove that GA is successfully conjugated to the Chi chain backbone.

OHA was synthesized by oxidizing HA with sodium periodate ($NaIO_4$) (Figure S4a, Supporting Information). In the ^1H NMR spectra (Figure S4b, Supporting Information), compared with HA, OHA has new chemical shifts at 4.838, 4.940, and 5.044 ppm. The signals should be allocated to hemiacetalic protons formed from aldehyde groups and neighboring hydroxyl groups, and are also direct evidences for the presence of aldehyde groups in the oxidized HA molecules.[34] More evidences can be found in the FTIR spectra of HA and OHA (Figure S4c, Supporting Information). There is a new peak at 1747 cm^{-1} in the spectrum of OHA sample, which is the characteristic peak of aldehyde groups.[35] In a word, the successful preparation of OHA is proved by ^1H NMR and FTIR results.

A hydrogel without hyBMSC-Exos was formed by mixing 3% (w/v) Chi-GA and 4% (w/v) OHA solution in a volume ratio of 10 : 1 and named as CG-OHA hydrogel. Similarly, a hydrogel containing 100 μg mL^{-1} hyBMSC-Exos was perpared and marked as CG-OHA@Exo hydrogel. Unless otherwise indicated, an used hydrogel solution in this study consisted of the hydrogel without being freeze-dried and with being suspended in culture medium, PBS or distilled water (18.25 MΩ cm) at a final concentration of 1 mg mL^{-1}. Micro-topology of freeze-dried CG-OHA and CG-OHA@Exo samples was observed by field emission scanning electron microscopy (FE-SEM). As exhibited in **Figure 2a**, they all have a typical 3D porous topology, and there is no significant difference in pore size and distribution. This implies that the incorporation of hyMSC-Exos has no impact on the microstructure of the hydrogel dressing. Indeed, exosomes do not exist in CG-OHA@Exo hydrogel only in the way of physical mixing, but participate in the formation of hydrogel networks. Covalent binding is formed between amino groups of exosomes' transmembrane proteins and phenolic hydroxyl groups of GA or aldehyde groups of OHA (Figure 1).[23] FTIR analysis was further performed to understand the key chemical bonds inside the hydrogels (Figure 2b). All the characteristic peaks (i.e., 1747, 1634, 1593, and 1544 cm^{-1}) belonging to OHA and Chi-GA appear in FTIR spectra of CG-OHA and CG-OHA@Exo samples. Strong absorption peak of 1634 cm^{-1} may be caused by the overlap of C = O stretching vibration and -C = N- stretching vibration.[30b,31,36] From energy dispersive X-ray spectroscopy (EDS) maps and X-ray photoelectron spectroscopy (XPS) results (Figure S5, Supporting Information), carbon (C), nitrogen (N), and oxygen (O) are the major elements of CG-OHA and CG-OHA@Exo samples. Sulfur (S) can be considered as a characteristic element of exosomes, which is mainly due to the sulfur-containing amino acids in exosomal proteins.

2.3. Multifunctional Properties of CG-OHA and CG-OHA@Exo Hydrogels

As a diabetic wound dressing, a hydrogel should not only have great physical properties such as needs-satisfying rheological property, great injectivity, excellent moldability, and strong swelling, but also display outstanding biological properties such as low hemolysis ratio, first-class antibacterial performance, preeminent antioxidant ability, and satisfactory biocompatibility. In this study, rheological properties of CG-OHA and CG-OHA@Exo materials were investigated by rheological tests under set conditions. Storage modulus (G') of the hydrogels is always greater than their loss modulus (G″) when angular frequency increases gradually from 0.1 to 100 rad s^{-1} (Figure 2c). This suggests that the hydrogels have great mechanical properties and fulfill the requirements of various diabetic wounds for a qualified dressing. Solid-liquid critical points of CG-OHA and CG-OHA@Exo hydrogels are 175% and 160% strain, respectively (Figure 2d). Next, the relationship between oscillation stress and oscillation strain of two kinds of hydrogels was observed (Figure 2e). Once oscillation strain is greater than 80%, oscillation stress of the hydrogels immediately drops to ≈50% of the maximum value. Since then, even if the strain increases to 1000%, the stress has been maintained at ≈600 Pa. We speculate that more than 80% strain is likely to break some hydrogen bonds and covalent bonds in

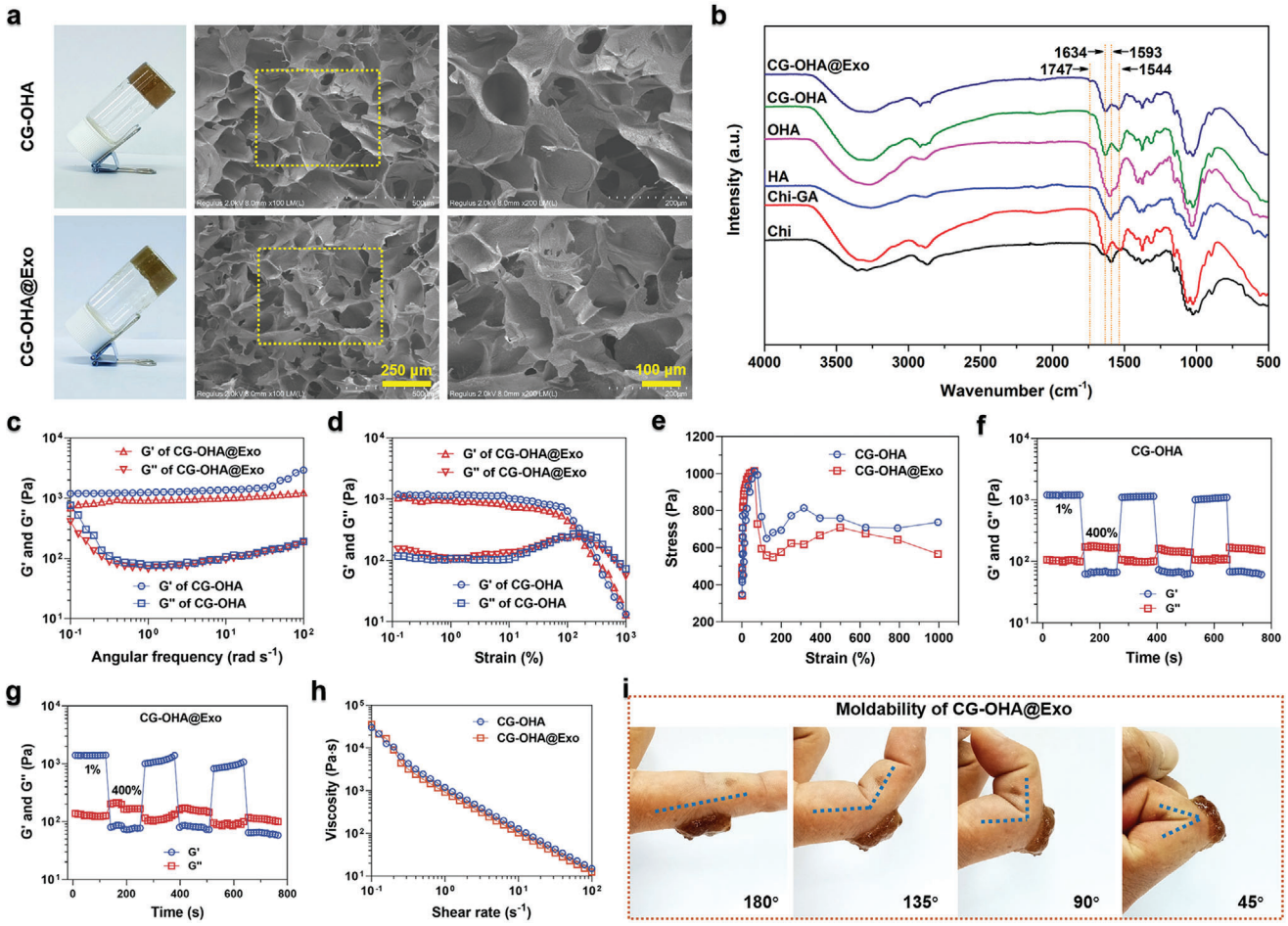

Figure 2. Physicochemical characteristics of CG-OHA and CG-OHA@Exo hydrogels. a) Representative photographs and FE-SEM images of the hydrogels. b) FTIR spectra of Chi, Chi-GA, HA, OHA, CG-OHA and CG-OHA@Exo samples. c) G' and G'' of the hydrogels on strain sweep from 0.1 to 100 rad s^{-1}. d) G' and G'' of the hydrogels when the strain continuously increases from 0.1% to 1000%. e) Oscillation stress-strain curves of 2 kinds of hydrogels. G' and G'' of CG-OHA f) and CG-OHA@Exo g) hydrogels when alternate step strain is switched from 1% to 800% with 3 times recycle. h) Shear thinning test of CG-OHA and CG-OHA@Exo hydrogels. i) Moldability of CG-OHA@Exo hydrogel. 200 μL of the hydrogel is applied to the second joint of an index finger, and then macro morphological changes of the hydrogel are observed as the joint changes to different angles.

hydrogels, but their self-healing ability keeps the hydrogels from breaking. This also indirectly shows that the hydrogels exhibit excellent self-healing property, which has been proved by a dynamic step-strain test (Figure 2f,g). Further, we investigated injectivity and moldability of CG-OHA and CG-OHA@Exo hydrogels. As shown in Figure 2h, the viscosity of the hydrogels decreases with the increasing of shear rate from 0.1 to 100 s^{-1}, which confirms the great injectable property of those two kinds of hydrogels (Movie S1, Supporting Information). And CG-OHA@Exo hydrogel that adheres to the index finger joint can maintain its original state at different angles and closely fits the skin (Figure 2i; Movie S2, Supporting Information). To evaluate the swelling properties of CG-OHA and CG-OHA@Exo hydrogels, gravimetry was used to determine the swelling ratios of the hydrogels in phosphate buffered saline (PBS; pH = 7.4) at 37 °C. As illustrated in Figure S6a (Supporting Information), the swelling ratios of CG-OHA and CG-OHA@Exo hydrogels increase gradually as the soaking time increases from 2 to 40 min. The swelling equilibrium state is reached at 40 min, and the swelling ratios of the hydrogels basically do not change even if the soaking time is increased to 240 min. The equilibrium swelling ratios (ESR) of CG-OHA and CG-OHA@Exo hydrogels are 1400.73 ± 77.25% and 1463.47 ± 117.20%, respectively (Figure S6b, Supporting Information). These results indicated that the hydrogels can swell well in PBS solution (pH = 7.4) at 37°C. In a word, both CG-OHA and CG-OHA@Exo hydrogels exhibit clinically desirable and excellent physical properties. And more notably, there is no significant difference in physical properties between CG-OHA and CG-OHA@Exo hydrogels, including rheological, self-healing, injectable, and swelling properties. This suggests that the introduction of hyBMSC-Exos does not significantly change the original physical properties of CG-OHA hydrogel, thus it may be suitable as a potential carrier of hyBMSC-Exos for the treatment of diabetic wounds.

Next, we evaluated basic biological properties of CG-OHA and CG-OHA@Exo hydrogels. As displayed in **Figure** 3a, except for positive control group (Triton X-100), the solution of the other groups is hardly observed to be red because only a tiny number of

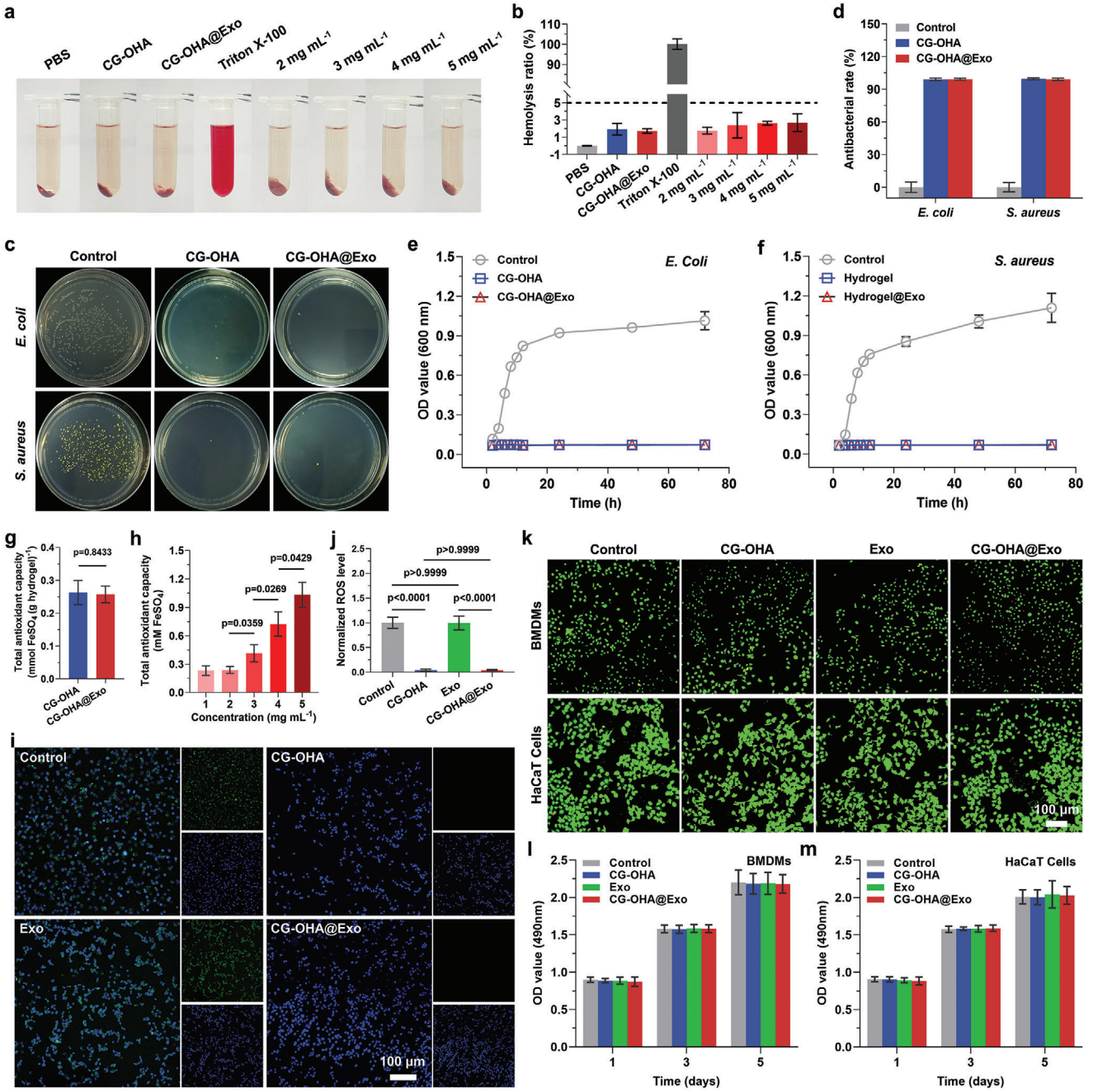

Figure 3. Basic biological properties of CG-OHA and CG-OHA@Exo hydrogels. a) Representative photographs of different hydrogels' hemolysis assay. Hemolysis characteristics of CG-OHA@Exo hydrogel's suspension with higher concentration (2, 3, 4, and 5 mg mL^{-1}) were also investigated. b) Hemolysis ratios of different hydrogels ($n = 3$). c) Representative photographs of re-cultivated *E. coli* and *S. aureus* colonies on sterile agar plates. d) Antibacterial efficiency of 2 kinds of hydrogels for *E. col* and *S. aureus* after 24 h cocultivation ($n = 5$). Growth curves of *E. coli* e) and *S. aureus* f) cocultured with CG-OHA and CG-OHA@Exo hydrogels' suspension for 72 h. g) Total antioxidant capacity of two kinds of hydrogels (n = 3). h) Total antioxidant capacity of CG-OHA@Exo hydrogel's suspension with different concentration (1, 2, 3, 4, and 5 mg mL^{-1}). i) Representative fluorescence images of BMDMs stained with DCFH-DA and DAPI after being treated by 100 μM H_2O_2 and different samples. j) Relative ROS level in BMDMs obtained by analyzing the fluorescence images ($n = 3$). k) Live/dead staining of BMDMs and HaCaT cells treated with PBS (Control), CG-OHA hydrogel, Exo, and CG-OHA@Exo hydrogel for 24 h. Cell viability of BMDMs l) and HaCaT cells m) treated with PBS (Control), CG-OHA hydrogel, Exo, and CG-OHA@Exo hydrogel for 24 h ($n = 3$). All quantitative data are presented as mean ± standard deviation (SD). If $p < 0.05$, the difference is considered statistically significant.

red blood cells are destroyed to release hemoglobin. Quantitative analysis indicates that CG-OHA@Exo hydrogel, even under the concentration of 5 mg mL^{-1}, shows significantly lower hemolysis ratio than the judging criterion (5%) for biomaterials with eligible hemocompatibility (Figure 3b).[22b] This fully confirms the point that CG-OHA@Exo hydrogel has excellent hemocompatibility. To investigate antibacterial ability of CG-OHA and CG-OHA@Exo hydrogels, two typical infectious organisms, namely, Staphylococcus aureus (*S. aureus*) and Escherichia coli (*E. coli*), were applied as representatives of Gram-positive and Gram-negative bacteria, respectively. In Figure 3c, compared with Control group, almost none of the bacteria survive in CG-OHA and CG-OHA@Exo groups after 24 h of co-culture. Antibacterial rates of two hydrogels are more than 98% (Figure 3d). It is found by observing the growth of *S. aureus* and *E. coli*, that the bacteria in CG-OHA and CG-OHA@Exo groups are almost completely killed in the first very short time, and there is no significant growth in the bacterial population during the next 72 h (Figure 3e,f). Underlying mechanisms of great antibacterial ability of those two hydrogels may lie in the following: (1) Chitosan itself has great antibacterial ability.[37] Protonated amino groups in chitosan molecules can neutralize negative charge on the surface of bacteria, in turn damaging the normal metabolism of the bacteria.[38] After being modified by gallic acid, it has also been confirmed to significantly inhibit bacterial proliferation via destroying bacterial cell walls and membranes.[39] (2) It has been reported that the product (i.e., —C = N—) of Schiff base reaction between amino group and aldehyde group or phenol hydroxyl group exhibits excellent antibacterial effect.[38,40] Because of excessive inflammation and hyperglycemic state, diabetic wounds are subjected to high oxidative stress, which results in cellular damage and further exacerbates inflammation, in turn prolonging wound healing.[22b,41] Our previous studies demonstrated that pathophysiological base of high oxidative stress is reactive oxygen species (ROS) overproduction and insufficient antioxidant systems.[22b,42] In the present study, therefore, we have designed a hydrogel dressing with ROS scavenging property for attenuating high oxidative stress of diabetic wounds. As exhibited in Figure 3g, total antioxidant capacity of those two kinds of hydrogels is 0.263 ± 0.036 and 0.257 ± 0.025 mmol $FeSO_4$ (g hydrogel)$^{-1}$, respectively. And total antioxidant capacity of CG-OHA@Exo hydrogel suspension is positively correlated with its concentration (Figure 3h). Also, significant reduction of ROS level in high-glucose exposed Bone marrow-derived macrophages (BMDMs) after 48 h of treatment with CG-OHA or CG-OHA@Exo hydrogels when compared with Control and Exo groups ($p < 0.0001$) (Figure 3i,j). There is no significant difference in ROS levels between CG-OHA and CG-OHA@Exo groups (Figure 3i,j), indicating that the addition of hyBMSC-Exos has little effect on the antioxidant property of CG-OHA hydrogel. To investigate the cytocompatibility of Exo as well as CG-OHA and CG-OHA@Exo hydrogels, BMDMs and HaCaT cells were respectively co-cultured with the samples for a pre-set time, and then live/dead cell staining and MTS assay were performed. The results show that BMDMs and HaCaT cells treated with these three kinds of samples exhibit similar cell viability when compared with those of Control group (without treatment) (Figure 3k,l,m). Collectively, CG-OHA@Exo hydrogel displays outstanding basic biological properties, including low hemolysis ratio, first-class antibacterial performance, significant antioxidant potential, and great cytocompatibility, indicating that the hydrogel can act as an extracellular matrix for contacting cutaneous tissue directly.

2.4. Degradation of Hydrogels and Release Behaviors of hyBMSC-Exos

Although exosomes possess considerable medical prospects, their rapid clearance and inactivation in vivo after administration hamper their clinical applications.[43] Therefore, exosome-based application is a dose-dependent pattern.[44] Many basic and clinical studies tend to maintain local concentration of exosomes by multiple dose regimen, but it is still bound by the cost of exosomes preparation as well as the pain and discomfort of injection. For that reason, we opted to embed hyBMSC-Exos into CG-OHA hydrogel to achieve in situ sustained release of the exosomes at diabetic wound sites. First of all, the in vivo degradation of CG-OHA and CG-OHA@Exo hydrogels was observed to determine whether CG-OHA hydrogel has the potential to slow release hyBMSC-Exos. As shown in Figure S7a (Supporting Information), only a small number of CG-OHA and CG-OHA@Exo hydrogels remain in the wounds and the unhealed wounds are exposed after 96 h of administration. And the weight of the residual hydrogels does not exceed 10 mg (Figure S7b, Supporting Information).

Further, BCA protein assay and in vivo optical imaging were performed to investigate the release behaviors of hyBMSC-Exos from CG-OHA@Exo hydrogel, which would also help us to indirectly understand the degradation of the hydrogel. As presented in **Figure** 4a,b, CG-OHA@Exo hydrogel exhibits a long term and sustained exosome-releasing profile in vitro, which is fully supported by the result of BCA assay for exosome-derived protein concentration (Figure 4c). In vivo, when hyBMSC-Exos are dispersed into PBS alone for administration, almost no exosomes can be observed in the wounds 48 h later (Figure 4d). In contrast, there is still significant exosome signaling in the wounds of CG-OHA@Exo group at 96 h after a single dose (Figure 4d). The percentages of exosomes remaining in the wounds of Exo and CG-OHA@Exo groups are 22.7 ± 5.70% and 80.9 ± 5.34% at 48 h, while those are 1.76 ± 2.74% and 37.8 ± 1.70% at 96 h (Figure 4e). These results can also be corroborated by the experimental results of hydrogel degradation in vivo (Figure S7, Supporting Information).

Possible reasons of CG-OHA@Exo hydrogel enhancing the stability of hyBMSC-Exos and slowing down their release in the wounds are as follows: (1) The amino groups of transmembrane proteins on the exosome surface participates in the formation of covalent bonds and a part of hyBMSC-Exos are thus fixed into CG-OHA@Exo hydrogel (Figure 1).[23] The water in the hydrogel may take part in the formation of hydrogel networks by forming hydrogen bonds (Figure 1).[22b] Therefore, although another part of the exosomes still remain free in the solvent of the hydrogel, they do not explode into the wound. When the hydrogel is degraded, the loaded exosomes will be gradually released into the wound environments. (2) The hydrogel undergoes a slow degradation process. It takes at least four days for the hydrogel to completely degrade (Figure S7, Supporting Information). This not only slows the rate of the exosomes entering the wound

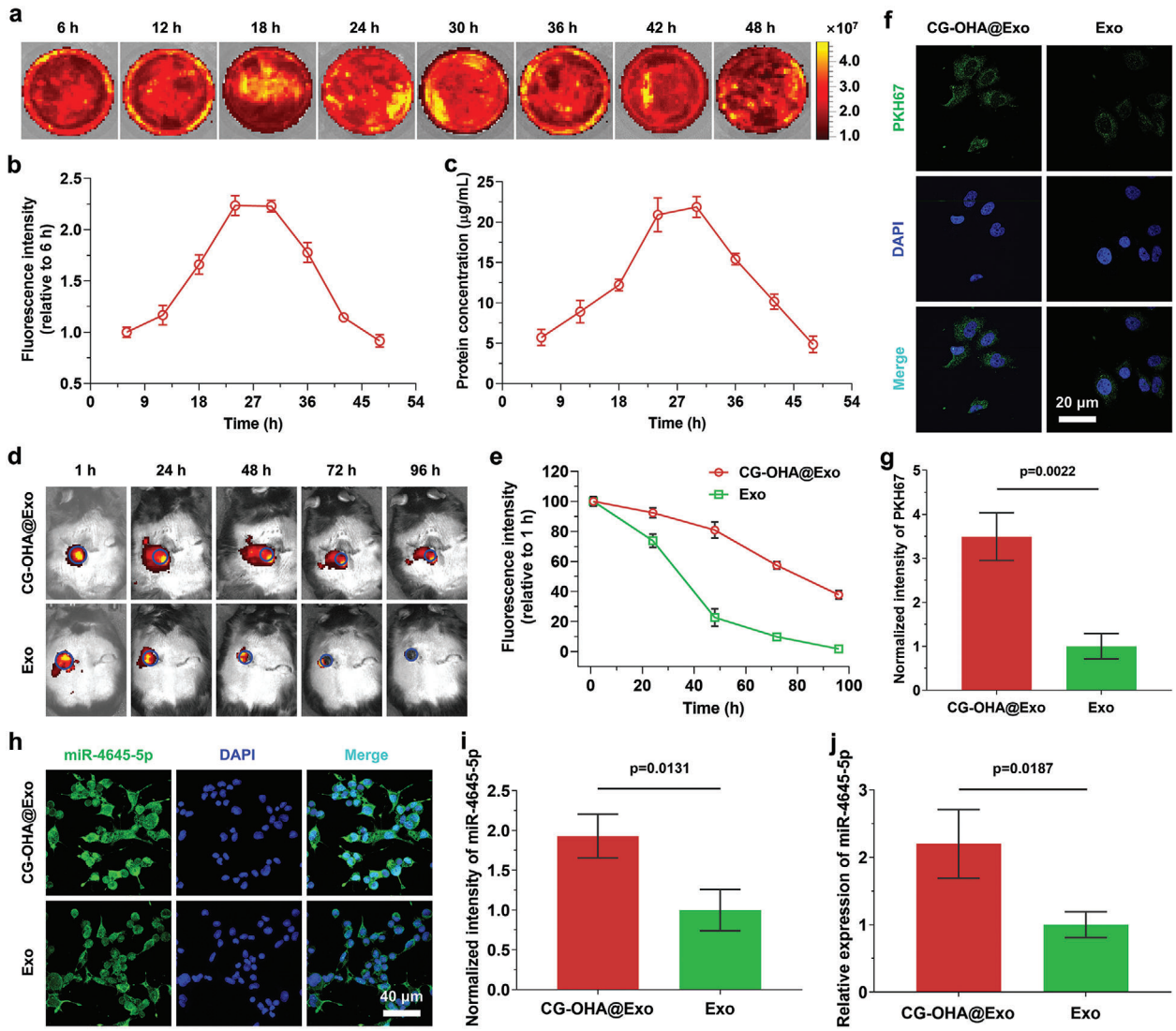

Figure 4. Exosome stability and release of CG-OHA@Exo hydrogel as well as exosome uptake by BMDMs. a) Exosome release profiles from CG-OHA@Exo hydrogel in real time obtained by an In Vivo Imaging System (IVIS). 1,1-dioctadecyl-3,3,3,3-tetramethylindotricarbocyaine iodide (DiR) was used to label exosomes. b) Fluorescence intensity at different time points within 48 h relative to 6 h ($n = 3$). c) The concentration of exosome-derived proteins within 48 h ($n = 3$). d) In vivo investigation of exosome stability and release in different ways of administration. DiR was used to label exosomes. e) Fluorescence intensity at different time points within 96 h relative to 1 h ($n = 3$). f) Representative immunofluorescence images of PKH67 (green) and nuclei (blue) in BMDMs at 48 h after co-culture with free hyBMSC-Exos or CG-OHA@Exo hydrogel. g) Normalized fluorescence intensity of PKH67 obtained by analyzing the immunofluorescence images ($n = 3$). h) Representative immunofluorescence images of miR-4645-5p (green) and nuclei (blue) in BMDMs at 48 h after co-culture with free hyBMSC-Exos or CG-OHA@Exo hydrogel. i) Normalized fluorescence intensity of miR-4645-5p obtained by analyzing the immunofluorescence images ($n = 3$). j) Relative mRNA level of miR-4645-5p in BMDMs at 48 h after co-culture with free hyBMSC-Exos or CG-OHA@Exo hydrogel ($n = 3$). All quantitative data are presented as mean ± SD. If $p < 0.05$, the difference is considered statistically significant.

environments, but also physically prevents the exosomes from prematurely interacting with other substances in the wounds.

The above results indicate that CG-OHA@Exo hydrogel can enhance in vitro and *vivo* retention of hyBMSC-Exos through exquisite control of exosome release.

2.5. Exosome Uptake by Target Cells

In fact, biological impact of exosomes depends on transmitting functional components directly into recipient cells.[45] Herein, we conducted the investigation of exosome uptake by targeted cells. Immunofluorescence analysis shows that BMDMs treated by CG-OHA@Exo hydrogel display significantly higher exosome uptake than those incubated with free exosomes ($p = 0.0022$) (Figure 4f,g). Although there are no direct evidences that hydrogels can mediate exosomes to bind with cells and be taken up, we speculate that slow-release effect of CG-OHA@Exo hydrogel on hyBMSC-Exos may be an important contributor to easier uptake of the exosomes by BMDMs. According to the results of recent studies, exosome internalization is the principal method for exosome uptake,[46] which depends on exosomes'

surface proteins.[47] Several studies have shown that tetraspanin membrane proteins, such as CD9 and CD81, facilitate exosome uptake.[48] Others have also suggested that the composition of lipids and glycans on exosomes may determine the target cell tropism of exosomes.[49] It is tempting to speculate that exquisite control of exosomes release with hydrogels may be efficacious in maintaining membrane integrality of exosomes in the extracellular environments and thus avoiding the proteolytic cleavage and destruction of lipids and glycans on exosomes.

As noted above, exosome bioactivity plays an important role in exosome-based regenerative therapies. Exosomes-derived microRNAs (miRNAs) are well considered to be one of the primary functional components of exosomes and responsible for regulating biological function of target cells.[50] Meanwhile, exosomes act as the carrier for miRNAs with the ability to overcome many challenges, such as chemically instability, limited tissue targeting of miRNAs, as well as extracellular and intracellular barriers.[51] Exosome instability leads to low amounts of specific miRNAs from exosomes in targeted cells, which also means exosome inactivation. In our previous study, miR-4645-5p was found to be a main functional molecular carried by hyBMSC-Exos to regulate epidermal autophagy via inhibiting mitogen activated protein kinase activated protein kinase 2 (MAPKAPK2).[16b] Therefore, the expression of miR-4645-5p in BMDMs were employed to further investigate the uptake efficiency of hyBMSC-Exos by BMDMs. The cells treated with CG-OHA@Exo hydrogel present significantly enhanced fluorescence in comparison with those treated with free exosomes ($p = 0.0131$) (Figure 4h,i). Quantitative real-time polymerase chain reaction (RT-qPCR) results also indicate miR-4645-5p expression level of BMDMs in CG-OHA@Exo group is significantly higher than that in Exo group ($p = 0.0187$) (Figure 4j).

Overall, CG-OHA@Exo hydrogel can serve as an excellent carrier for hyBMSC-Exos because it can significantly improve the stability of exosomes, achieve sustained slow release of exosomes at wound sites, and improve the uptake efficiency of exosomes by target cells.

2.6. In Vivo Diabetic Wound Healing

Full-thickness diabetic wound models were established on 8-week-old male db/db diabetic mice to investigate the ability of CG-OHA@Exo hydrogel accelerating diabetic wound healing (**Figure 5**a). As illustrated in Figure 5b,c, the wounds treated by CG-OHA@Exo hydrogel display the fastest healing rate than those of the other groups. Four days after administration, the area of the wounds in CG-OHA@Exo group has been reduced to ≈60% of its original size, and the wounds have healed almost completely at day 14 after treatment (Figure 5d). By contrast, the group administered with free hyBMSC-Exos shows a much slower rate of wound healing, with ≈15% of unhealed wounds at day 14 (Figure 5d). Notably, there is no significant difference in wound healing rate between Control and CG-OHA groups (Figure 5b,c,d).

H&E and Masson trichrome staining was conducted to observe the difference of wound healing among all groups from a histological point of view. At day 6 post-wounding, the formation of thin epidermal tissue can be observed in wounds treated with PBS or CG-OHA hydrogel (Figure 5e), and the epidermal thickness is ≈30 μm (Figure 5f). Better epidermal regeneration appears in the wounds of Exo group, while the wounds treated with CG-OHA@Exo hydrogel show the most epidermal regrowth when compared with the other three groups (Figure 5e). The thickness of newly formed epidermis in the wounds of the two groups reaches 56.0 ± 4.82 and 90.0 ± 6.87 μm, respectively (Figure 5f). Similar trends of dermal tissue regeneration can be observed (Figure 5e,g). Another biological event that defines wound regeneration is collagen synthesis and deposition, which has been well-recognized as a symbolic event of the remodeling phase. A commonly accepted view is that proper collagen synthesis and deposition is beneficial for improving the tensile strength of newly formed skin tissue, thus accelerating the functional recovery of the tissue.[52] In this study, the results of Masson trichrome staining at day 10 post-wounding show significantly more regular, more orderly, and denser collagen arrangement in CG-OHA@Exo group than that in the other three groups (Figure 5e).

All the above results indicate that CG-OHA@Exo hydrogel has an active help in the regulation of re-epithelialization, dermal tissue regeneration, as well as order arrangement and deposition of collagen, thus leading to an accelerated and superior diabetic wound healing. In addition, from the difference of wound healing among the four groups, we can also conclude that CG-OHA hydrogel has no significant promoting effect on diabetic wound healing, while hyBMSC-Exos may be the most important factor in CG-OHA@Exo hydrogel showing an excellent ability to promote diabetic wound healing. The underlying mechanisms are worth further investigation.

2.7. Underlying Causes of Diabetic Wound Healing Promoted by CG-OHA@Exo Hydrogel

The current consensus is that diabetic wounds are characterized by chronic inflammation and dramatically inhibited angiogenesis.[22b,53] Macrophage polarization dysregulation is considered to be among the major mechanisms responsible for persistent inflammatory response and impaired revascularization.[22b,54] Therefore, in a simulated diabetes microenvironment (25 mM glucose and 100 ng mL^{-1} lipopolysaccharide (LPS)), we investigated the beneficial effect of CG-OHA@Exo hydrogel on the regulation of macrophage polarization. After co-incubation for 48 h, macrophage subtypes were sorted and identified by Fluorescence Activated Cell Sorting (FACS). As exhibited in **Figure 6**a,b, more than 50% of BMDMs are M1 macrophages (inducible nitric oxide synthase $(iNOS)^+/CD80^+$) in Control and CG-OHA groups when compared with those in Exo and CG-OHA@Exo groups. At the same time, it is found that the percentage of M2 phenotype macrophages (arginase 1 $(Arg1)^+/CD206^+$) in CG-OHA@Exo hydrogel treated cells is more than 60% (Figure 6c,d). We also demonstrated mRNA and protein levels of M1 macrophage marker (i.e., iNOS) are observably inhibited in Exo and CG-OHA@Exo groups, and the down-regulated iNOS level is the most remarkable in CG-OHA@Exo group (Figure 6e,g–i; Figure S8, Supporting Information). Moreover, the results of RT-qPCR and western blotting indicate the significant increase

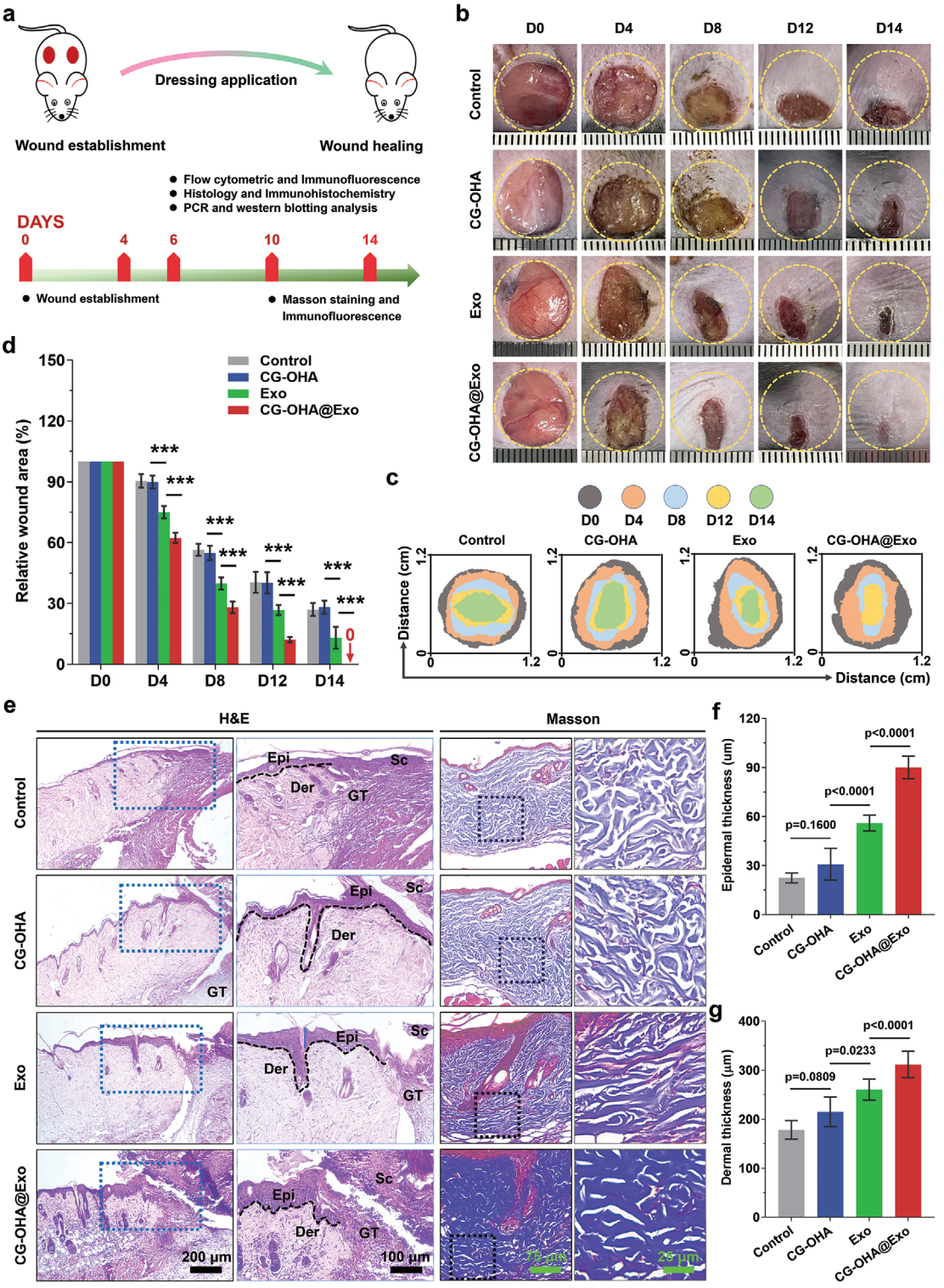

Figure 5. In vivo evaluation of diabetic wound healing evaluation. a) A schematic diagram illustrating the timeline of in vivo study. Two circular full-thickness excisional wounds with 1 cm in diameter were created on the back of db/db mice. b) Representative optical photographs of the wounds at day 0, 4, 8, 12, and 14 after surgery. c) Traces of wound-bed closure during 14 days. d) Relative wound area of Control (PBS treatment), CG-OHA, Exo, and CG-OHA@Exo groups at day 0, 4, 8, 12, and 14 post-wounding ($n = 6$). e) Representative H&E and Masson trichrome staining images obtained from wound sites of the four groups. At day 6 after surgery, some mice in each group were euthanized, and newly formed skin tissue was collected to perform H&E staining. Masson trichrome staining was also conducted at day 10 post-wounding. Quantitative thickness of epidermal f) and dermal g) tissues at day 6 after surgery ($n = 6$). All quantitative data are presented as mean ± SD. ***$p < 0.001$. If $p < 0.05$, the difference is considered statistically significant. Epi: epidermis, Der: dermis, GT: granulation tissue, Sc: scab.

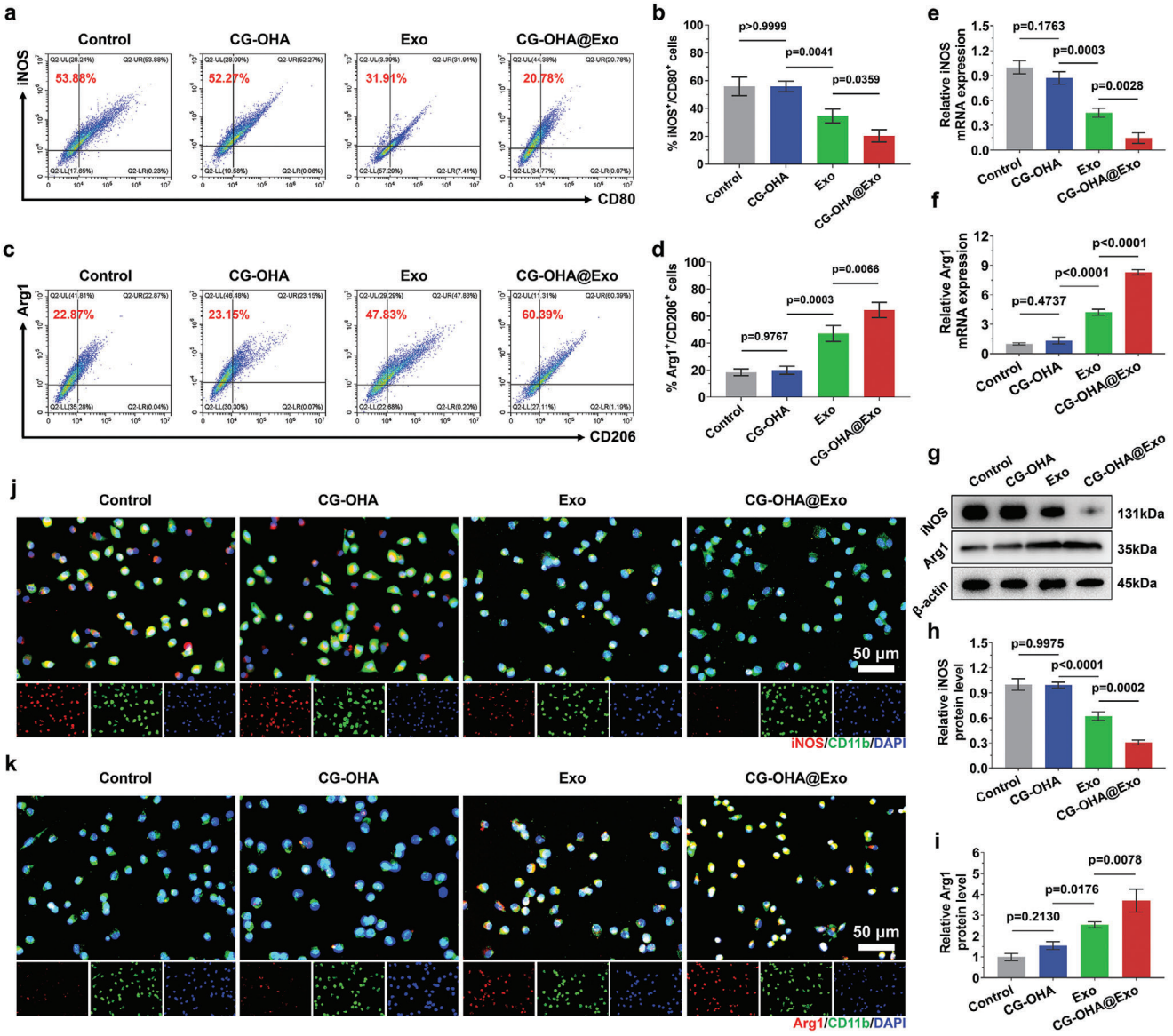

Figure 6. In vitro macrophage polarization regulated by hyBMSC-Exos as well as CG-OHA and CG-OHA@Exo hydrogels. a) M1 phenotype macrophages sorted and identified by FACS after BMDMs were treated with CG-OHA hydrogel, free hyBMSC-Exos, and CG-OHA@Exo hydrogel for 48 h. b) The percentage of iNOS$^+$/CD80$^+$ macrophages ($n = 3$). c) M2 phenotype macrophages sorted and identified by FACS after BMDMs were treated with CG-OHA hydrogel, free hyBMSC-Exos, and CG-OHA@Exo hydrogel for 48 h. d) The percentage of Arg1$^+$/CD206$^+$ macrophages ($n = 3$). Relative mRNA level of iNOS e) and Arg1 f) in the BMDMs treated with CG-OHA hydrogel, free hyBMSC-Exos, and CG-OHA@Exo hydrogel for 48 h ($n = 3$). g) Western blotting assay of iNOS and Arg1 after co-culture of cells and materials for 48 h. Quantitative western blotting data showing the expression level of iNOS h) and Arg1 i) by analyzing the bands in (g) ($n = 3$). j) Representative immunofluorescence images of iNOS (red), CD11b (green), and nuclei (blue) in the BMDMs treated with CG-OHA hydrogel, free hyBMSC-Exos, and CG-OHA@Exo hydrogel for 48 h. k) Representative immunofluorescence images of Arg1 (red), CD11b (green), and nuclei (blue) in the BMDMs treated with CG-OHA hydrogel, free hyBMSC-Exos, and CG-OHA@Exo hydrogel for 48 h. All quantitative data are presented as mean ± SD. If $p < 0.05$, the difference is considered statistically significant.

of M2 macrophage marker (i.e., Arg1) in the BMDMs treated with CG-OHA@Exo hydrogel when compared with that in the cells incubated with CG-OHA hydrogel and free hyMSC-Exos (Figure 6f,g–i; Figure S8, Supporting Information). Additionally, the co-expression of Arg1 and CD11b is ubiquitous in the BMDMs subjected to CG-OHA@Exo hydrogel, while the co-expression of iNOS and CD11b is significantly reduced (Figure 6j,k; Figures S9 and S10, Supporting Information).

To further investigate whether CG-OHA@Exo hydrogel leads to changes in infiltration or phenotype of skin wound macrophages, we analyzed the type of macrophages in different wounds. Total number of the target cells (CD11b$^+$/F4/80$^+$ cells) is ≈13 500 in each group (**Figure** 7a). Flow cytometric quantitation of sorted macrophages from CG-OHA@Exo hydrogel treated wounds at day 6 post-wounding, shows a significant increase in M2 phenotype macrophages (Arg1$^+$/CD206$^+$

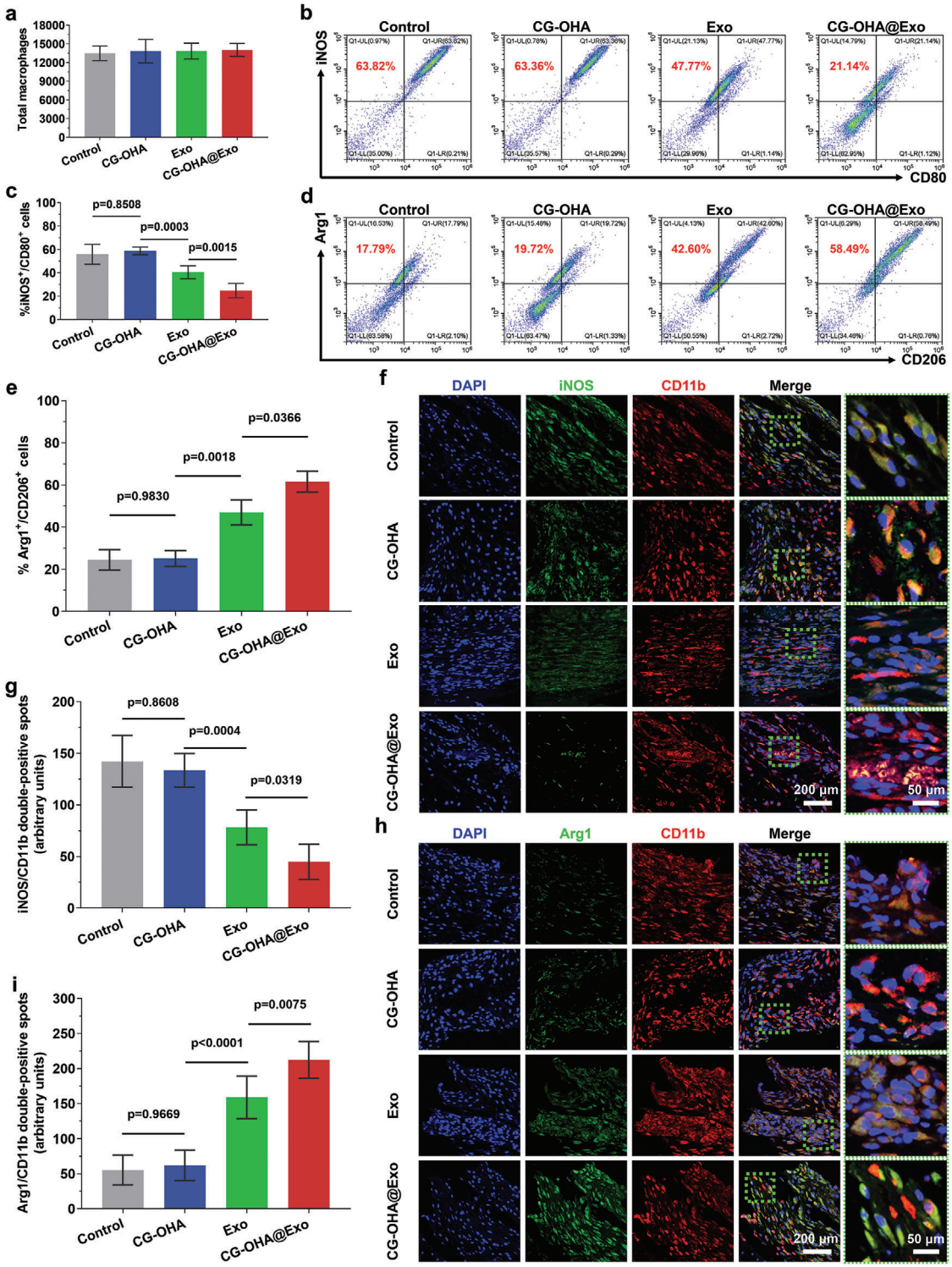

Figure 7. In vivo macrophage polarization regulated by hyBMSC-Exos as well as CG-OHA and CG-OHA@Exo hydrogels. a) Total number of the sorted macrophages collected from four kinds of wound sites at day 6 post-wounding ($n = 6$). b) M1 phenotype macrophages sorted and identified by FACS. c) The percentage of $iNOS^+/CD80^+$ macrophages ($n = 6$). d) M2 phenotype macrophages sorted and identified by FACS. e) The percentage of $Arg1^+/CD206^+$ macrophages ($n = 6$). f) Representative immunofluorescence images of iNOS (green), CD11b (red), and nuclei (blue) in granulation tissue of the four groups at day 6 after surgery. g) Quantitative iNOS/CD11b double-positive spots obtained by analyzing the immunofluorescence images ($n = 6$). h) Representative immunofluorescence images of Arg1 (green), CD11b (red), and nuclei (blue) in granulation tissue of the four groups at day 6 after surgery. i) Quantitative Arg1/CD11b double-positive spots obtained by analyzing the immunofluorescence images ($n = 6$). All quantitative data are presented as mean ± SD. If $p < 0.05$, the difference is considered statistically significant.

cells), along with a reduction of M1 phenotype macrophages (iNOS$^+$/CD80$^+$ cells) (Figure 7b–e). The *in situ* distribution of different macrophages in wounds was observed by immunofluorescence staining. As shown in Figure 7f–i, iNOS$^+$/CD11b$^+$ cells (M1 phenotype macrophages) are abundant throughout the wounds of Control and CG-OHA groups, while M2 phenotype macrophages with a remarkable rise of Arg1/CD11b co-expression are more widely distributed in the wounds of CG-OHA@Exo group. The above results suggest that CG-OHA@Exo hydrogel displays superior effects in inhibiting LPS and high glucose induced M1 macrophage polarization and promoting the increased transition of M1-to-M2 macrophage polarization.

Next, we observed the effects of M1-to-M2 macrophage polarization on inflammatory response and angiogenesis in the diabetic wounds. It is reported that inflammatory response is closely associated with macrophages-derived cytokines.[55] Therefore, we firstly investigated mRNA expression levels of pro-inflammatory factors (i.e., IL-1β, IL-6, IL-12, and IL-23) from M1 macrophages and anti-inflammatory cytokines (i.e., IL-10 and TGF-β1) from M2 macrophages. CG-OHA@Exo hydrogel and free hyMSC-Exos significantly inhibit the expression of proinflammatory factors in the BMDMs, and the downregulation of four kinds of genes in CG-OHA@Exo group is more remarkable than that in Exo group ($p < 0.05$ or $p < 0.001$) (**Figure 8**a,b; Figure S11a,b, Supporting Information). Completely opposite trends of anti-inflammatory cytokine expression can be observed (Figure 8c; Figure S11c, Supporting Information). In addition, mRNA expression levels of pro-inflammatory factors and anti-inflammatory cytokines from wound-infiltrating macrophages were also detected at day 6 post-wounding. Compared with the other groups, the expression of anti-inflammatory cytokines in wound-infiltrating macrophages from the wounds of CG-OHA@Exo group is significantly increased, while the level of canonical inflammatory cytokines is dramatically decreased. This also verifies the suppression of inflammation in diabetic wounds upon CG-OHA@Exo hydrogel treatment (Figure S12, Supporting Information). To find out whether the increased mRNA expression of the above cytokines in the treated BMDMs leads to higher secretion levels of corresponding proteins, enzyme linked immunosorbent assay (ELISA) was used to detect the concentration of the cytokines in culture supernatant. The results generally correspond with those of RT-qPCR, that is, only a small number of proinflammatory factors are expressed in the BMDMs treated with CG-OHA@Exo hydrogel, while the secretion of anti-inflammatory factors increases by several or even a dozen times than that of Control group (Figure 8d–f; Figure S13, Supporting Information). To sum it up, CG-OHA@Exo hydrogel can inhibit inflammatory response through shifting macrophage polarization from a pro-inflammatory phenotype (M1) to an anti-inflammatory phenotype (M2).

The proliferative phase of wound healing is characterized by granulation tissue formation in wounds, which requires the invasion of endothelial cells followed by the occurrence of neovascularization to ensure the transport of nutrients and oxygen.[56] Promoting angiogenesis is another universally recognized effect of macrophage polarization toward M2 type.[22b,53] The underlying reason is that M2 macrophages can express a variety of pro-angiogenic factors.[22b] Among them, TGF-β1, in addition to participating in anti-inflammatory processes, can also promote vascular regeneration via inducing the expression of VEGF.[22b,57] VEGF is one of the most potent angiogenic factors. It can promote the migration and proliferation of vascular endothelial cells and accelerate the ripening of newly formed blood vessels.[22b,58] In this study, we are surprised to find that the expression trend of VEGF (whether mRNA or protein) in the BMDMs treated by CG-OHA hydrogel, free hyMSC-Exos, and CG-OHA@Exo hydrogel is strikingly similar to that of TGF-β1 observed above (Figure 8g,h), which is also fully supported by the results of RT-qPCR for wound-infiltrating macrophages at day 6 post-wounding (Figure S14, Supporting Information). Further, angiogenesis in diabetic wounds managed by different dressings was investigated at day 6 post-wounding. The wounds of Exo group exhibit an increasing expression of endothelial marker CD31 and angiogenesis-related protein α-smooth muscle actin (α-SMA) than CG-OHA and Control groups, whereas CG-OHA@Exo group has more extensive CD31 and α-SMA staining in wound beds when compared with Exo group (Figure 8i–l).

Cumulatively, following a significant switch of M1-to-M2 macrophage polarization in diabetic wounds treated with CG-OHA@Exo hydrogel, the macrophages that returned to normal function do everything they should do, including relieving persistent wound inflammation and rebuilding rich vascular system, in turn accelerating re-epithelialization and collagen deposition until wound healing.

2.8. Underlying Molecular Mechanism of Macrophage Polarization Regulated by CG-OHA@Exo Hydrogel

A recent study shows that SREBP2-driven transcriptional response contributes to M1 macrophage polarization and inflammatory response, and SREBP2 inhibition can accelerate wound healing associated with a shift in macrophage polarization toward M2 phenotype.[59] SREBP2 undergoes proteolytic cleavage in Golgi bodies after receiving environmental signals, followed by releasing an amino-terminal fragment (N-SREBP2, i.e., active SREBP2) for transport to the nucleus, where active SREBP2 binds to various inflammatory response genes and has transcriptional activity.[60] Therefore, we hypothesize the possibility that hyBMSC-Exos from CG-OHA@Exo hydrogel exert pro-macrophage polarization property via regulating SREBP2 activity.

To this end, we assessed SREBP-2 nuclear translocation in the BMDMs upon CG-OHA@Exo hydrogel treatment. BMDMs were treated with high glucose (25 mM glucose) and 100 ng mL^{-1} LPS. As expected, the protein level of active SREBP2 in Exo and CG-OHA@Exo groups is inhibited significantly when compared with that of Control group, and the down-regulated active SREBP2 level is the most remarkable in CG-OHA@Exo group (**Figure 9**a,b; Figure S15, Supporting Information). Consistent with the results of western blotting, immunofluorescence data of the cells indicate that CG-OHA@Exo group shows more significant inhibitory effect on SREBP-2 nuclear translocation than CG-OHA and Exo groups (Figure 9c). Studies have confirmed that TNF-α accumulation is responsible for macrophage-mediated inflammatory disease pathogenesis,[61] and the process is associated with TNF-α induced SREBP2 activation.[61b] In this work, we detected protein expression of TNF-α and MAPKAPK2

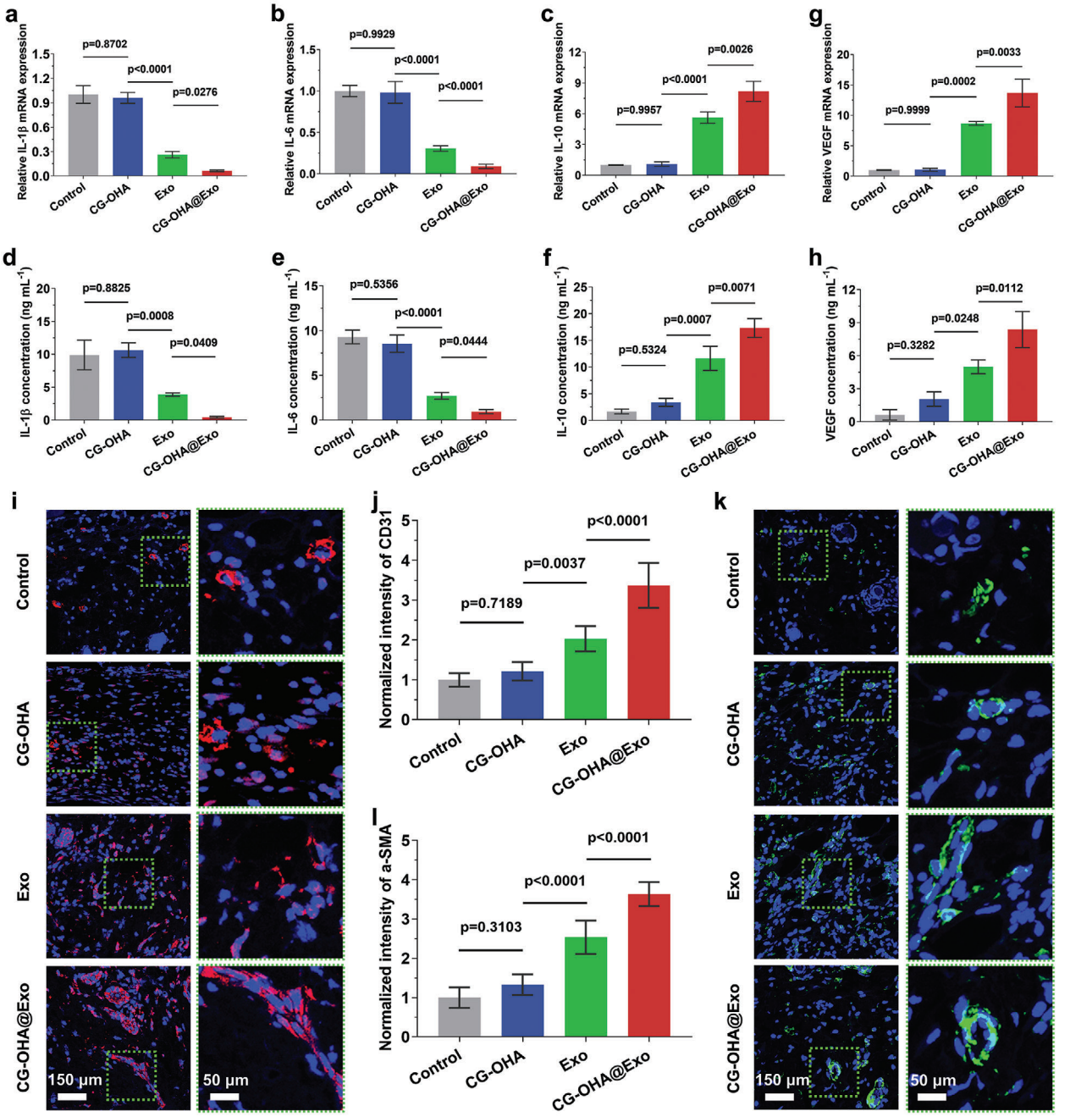

Figure 8. Biological events caused by macrophage polarization in diabetic wounds with the treatment of hyBMSC-Exos as well as CG-OHA and CG-OHA@Exo hydrogels. Relative mRNA level of IL-1β a), IL-6 b), and IL-10 c) in the BMDMs treated with CG-OHA hydrogel, free hyBMSC-Exos, and CG-OHA@Exo hydrogel for 48 h ($n = 3$). The concentration of IL-1β d), IL-6 e), and IL-10 f) secreted by polarized macrophages into culture medium at day 5 after treatment ($n = 3$). g) Relative mRNA level of VEGF in the BMDMs treated with CG-OHA hydrogel, free hyBMSC-Exos, and CG-OHA@Exo hydrogel for 48 h ($n = 3$). h) The concentration of VEGF secreted by polarized macrophages into culture medium at day 5 after treatment ($n = 3$). Representative immunofluorescence images i) and normalized fluorescence intensity j) of endothelial marker CD31 in granulation tissue at day 6 post-wounding. Representative immunofluorescence images k) and normalized fluorescence intensity l) of angiogenesis-related protein α-SMA in granulation tissue at day 6 post-wounding. All quantitative data are presented as mean ± SD. If $p < 0.05$, the difference is considered statistically significant.

to further gain insight into the mechanism of CG-OHA@Exo hydrogel regulating SREBP-2 activity in BMDMs. Western blotting analysis reveals the upregulated expression of TNF-α in Control group and the downregulated expression of TNF-α in Exo and CG-OHA@Exo groups (Figure 9d,e; Figure S16, Supporting Information). Similar trends of MAPKAPK2 expression can also be observed (Figure 9d,e; Figure S16, Supporting Information). In line with those findings, the work of Menon et al. found that MAPKAPK2 is an essential positive regulator of TNF-α biosynthesis at the post-transcriptional level by phosphorylating

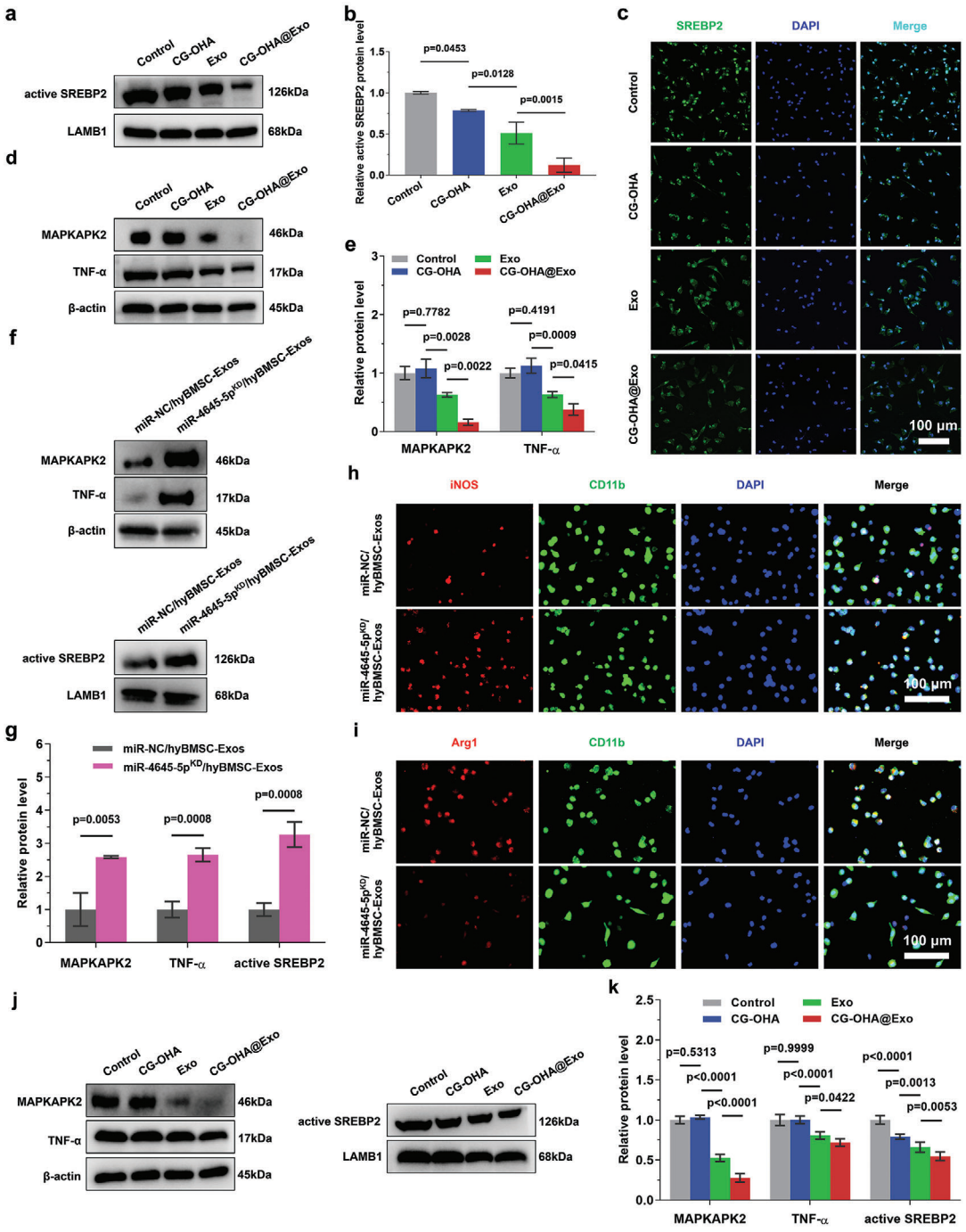

Figure 9. Underlying molecular mechanism of macrophage polarization regulated by CG-OHA@Exo hydrogel. a) Western blotting assay of active SREBP2 after co-culture of BMDMs and materials for 48 h. b) Quantitative western blotting data showing the expression level of active SREBP2 by analyzing the bands in (a) ($n = 3$). c) Representative immunofluorescence images of SREBP2 (green) and nuclei (blue) in the BMDMs treated with CG-OHA hydrogel, free hyBMSC-Exos, and CG-OHA@Exo hydrogel for 48 h. d) Western blotting assay of MAPKAPK2 and TNF-α after co-culture of cells and materials for 48 h. e) Quantitative western blotting data showing the expression level of MAPKAPK2 and TNF-α by analyzing the bands in (d) ($n = 3$). f) Western blotting assay of MAPKAPK2, TNF-α, and active SREBP2 in BMDMs treated with hyBMSC-Exos and miR-4645-5p gene-knockout hyBMSC-Exos for 48 h. g) Quantitative western blotting data showing the expression level of MAPKAPK2, TNF-α, and active SREBP2 by analyzing the bands in (f) ($n = 3$). h) Representative immunofluorescence images of iNOS (red), CD11d (green), and nuclei (blue) in the BMDMs treated with hyBMSC-Exos and miR-4645-5p gene-knockout hyBMSC-Exos for 48 h. i) Representative immunofluorescence images of Arg1 (red), CD11d (green), and nuclei (blue) in the BMDMs treated with hyBMSC-Exos and miR-4645-5p gene-knockout hyBMSC-Exos for 48 h. j) Western blotting assay of MAPKAPK2, TNF-α, and active SREBP2 in the wound-infiltrating macrophages treated with CG-OHA hydrogel, free hyBMSC-Exos, and CG-OHA@Exo hydrogel for 48 h. k) Quantitative western blotting data showing the expression level of MAPKAPK2, TNF-α, and active SREBP2 by analyzing the bands in (j) ($n = 3$). All quantitative data are presented as mean ± SD. If $p < 0.05$, the difference is considered statistically significant.

and inactivating the mRNA-destabilizing and translation-inhibiting tristetraprolin.[62] In a word, all the above results suggest that the inhibition of MAPKAPK2/TNF-α/SREBP2 signaling axis appears to be operative in transition of M1-to-M2 macrophage polarization upon CG-OHA@Exo hydrogel treatment.

Given the newly found function of hyBMSC-Exos-derived miR-4645-5p as a master negative regulator of MAPKAPK2 expression,[16b] we speculate that miR-4645-5p is responsible for M1-to-M2 macrophage polarization via inhibiting MAPKAPK2/TNF-α/SREBP2 signaling axis. To verify the hypothesis, we investigated how the exosomes derived from miR-4645-5p gene-knockout hyBMSCs induce macrophage polarization. The expression of miR-4645-5p in hyBMSCs is extremely low after gene knockout (Figure S17a, Supporting Information), and miR-4645-5p is hardly detectable in miR-4645-5p^{KD}/hyBMSC-Exos and miR-4645-5p^{KD}/hyBMSC-Exos treated BMDMs (Figure S17b,c, Supporting Information). The knockout of miR-4645-5p results in the activation of MAPKAPK2/TNF-α/SREBP2 signaling axis in BMDMs subjected to hyBMSC-Exos under a condition of high glucose (25 mM glucose) and LPS (100 ng mL^{-1}) (Figure 9f,g; Figure S18, Supporting Information), accompanied by the enhancement of M1 macrophage polarization (Figure 9h; Figure S19a, Supporting Information) and the inhibition of M2 macrophage polarization (Figure 9i; Figure S19b, Supporting Information). It can be seen that the shift of M1-to-M2 macrophage polarization upon hyBMSC-Exos treatment may be attributed to SREBP2 inactivation. This inspires us to address whether CG-OHA@Exo hydrogel also favors M2 macrophage polarization by regulating SREBP2 activation in vivo and SREBP2 activation is implicated in macrophage polarization dysregulation in diabetic wounds. At day 6 after surgery, free hyBMSC-Exos and CG-OHA@Exo hydrogel significantly downregulate intracellular levels of MAPKAPK2, TNF-α, and active SREBP2 in wound-infiltrating macrophages, whereas the downregulation of three kinds of proteins displays the most remarkable in CG-OHA@Exo group (Figure 9j,k; Figure S20, Supporting Information). The results indicate that the molecular mechanism of CG-OHA@Exo hydrogel in shifting macrophage polarization from M1 to M2 phenotype is to attenuate SREBP2 activation by transferring exosomal miR-4645-5p into macrophages for inhibiting MAPKAPK2 and TNF-α expression.

Regarding the difference in the expression of MAPKAPK2, TNF-α, and active SREBP2 among four groups, two points deserve special attention. On the one hand, CG-OHA@Exo hydrogel shows significantly better inhibitory effect on expression level of MAPKAPK2, TNF-α, and active SREBP2 than free hyBMSC-Exos, both in vitro and in vivo (Figure 9a–e,j,k). On the other hand, the expression of active SREBP2 in the BMDMs or the wound-infiltrating macrophages treated with CG-OHA hydrogel is significantly lower than that in Control group (Figure 9a–c,j,k), while there is no significant difference in MAPKAPK2 and TNF-α expression (Figure 9d,e,j,k). In addition to the fact that CG-OHA@Exo hydrogel can improve the stability of hyBMSC-Exos, slow down their release, and promote exosome uptake by target cells, we speculate that CG-OHA hydrogel has the ability of inhibiting SREBP2 activity independent of MAPKAPK2/TNF-α/SREBP2 signaling axis. A previous report has confirmed that ROS correlates with SREBP2 activation, and reducing ROS by overexpressing human copper-zinc superoxide dismutase can decrease active SREBP level in drosophila.[63] Considering that CG-OHA@Exo hydrogel has great antioxidant property (Figure 3g–j), it is tempting to speculate that the significant downregulation of active SREBP2 in the LPS-stimulated BMDMs treated with the hydrogel is most likely related to ROS scavenging. We experimentally addressed the possibility and found that ROS scavenging in the BMDMs with CG-OHA hydrogel and N-acetyl cysteine could contribute to SREBP2 inactivation (Figures S21 and S22, Supporting Information). However, there are no detectable differences in macrophage polarization and the progress of wound healing between Control and CG-OHA groups (Figures 5–7). It is possible that TNF-α stimulation may extend the genomic profile of SREBP2 binding to inflammatory response genes, in turn leading to macrophage polarization towards M1 phenotype. Supporting this possibility is the results of a previous report, that is, SREBP2 binding to inflammatory response genes is lower affinity, but the binding peaks are induced by TNF-α.[59] This suggests that only reducing active SREBP2 protein level without altering TNF-α expression, does not shift the balance of macrophage polarization from an inflammatory (M1) to a reparative phenotype (M2).

Overall, all the results support the notion that CG-OHA@Exo hydrogel exhibits excellent ability of relieving macrophage polarization dysregulation in diabetic wounds via inhibiting SREBP2 activity, which may be attributed to miR-4546-5p derived from hyBMSC-Exos in cooperation with antioxidant property of the hydrogel.

3. Conclusion

In this study, a multifunctional hydrogel on the basis of Chi-GA and OHA was successfully prepared as a carrier of hyBMSC-Exos to regulate macrophage phenotype switch during diabetic wound healing. The resulting hydrogel (CG-OHA@Exo hydrogel) not only has great physical properties such as needs-satisfying rheological property, good injectivity, great self-healing property, excellent moldability, and strong swelling, but also displays outstanding biological properties including low hemolysis ratio (1.71 ± 0.259% at 1 mg mL^{-1}), first-class antibacterial capacity (> 99% against *S. aureus* and *E. coli* at 1 mg mL^{-1}), preeminent antioxidant ability (0.232 ± 0.050 mmol $FeSO_4$ (g hydrogel)$^{-1}$ of total antioxidant capacity at 1 mg mL^{-1}), and satisfactory biocompatibility. Because covalent binding is formed between amino groups of exosomes' transmembrane proteins and phenolic hydroxyl groups of GA or aldehyde groups of OHA, the hydrogel enhances the stability of hyBMSC-Exos and slows down their release in diabetic wounds. It also dramatically improves the uptake efficiency of hyBMSC-Exos by BMDMs. Most importantly, CG-OHA@Exo hydrogel shows an excellent ability to promote diabetic wound healing by regulating macrophage polarization from an inflammatory to a reparative phenotype. The underlying molecular mechanism may be that miR-4546-5p derived from hyBMSC-Exos and antioxidant property of the hydrogel synergistically inhibit SREBP2 activity in macrophages. This work offers an alternative for developing a new-type multifunctional diabetic wound dressing.

4. Experimental Section

Cell Culture: BMSCs used in this study were purchased from the American Type Culture Collection (ATCC; Manassas, USA). The cells were incubated with a Mesenchymal Stem Cell Growth Kit for Bone Marrow-derived MSCs (ATCC PCS-500-041) (supplemented with 125 pg mL^{-1} recombinant human basic fibroblast growth factor (Sigma-Aldrich Co., St. Louis, USA), 15 ng mL^{-1} recombinant human insulin-like growth factor-1 (Sigma-Aldrich, USA), 7% fetal bovine serum (FBS; VivaCell, Shanghai, China) and 2.4 mM L-Alanyl-L-Glutamine (BioReagent; Sigma-Aldrich, USA)). BMSCs at 5th to 6th passage were chosen for further study. HaCaT cells were obtained from the Cell Bank/Stem Cell Bank of Chinese Academy of Sciences (Shanghai, China) and cultured in Minimum Essential Medium (Shanghai Chuanqiu Biotechnology Co., Ltd., China) containing 10% FBS and 1% penicillin-streptomycin (P/S) solution (100X; Gibco Co., Carlsbad, USA). BMDMs were isolated from mouse femurs and tibias. The entire procedure involving animal utilization was conducted in accordance with the regulations set by the Institutional Animal Care and Use Committee of China and was authorized by the Animal Ethics Committee of Shenzhen People's Hospital (Approval number: AUP-220516-SY-0242-01). After erythrocyte lysis with 0.17 M ammonium chloride, bone marrow cells were plated at a starting concentration of 10^5 cells mL^{-1} in LONSERA® Dulbecco's Modified Eagle Medium (Suzhou Shuangru Biotechnology Co., Ltd., Suzhou, China) supplemented with 10% heat-inactivated fetal calf serum (Merck Millipore, Berlin, Germany), 1% P/S, and 20% recombinant macrophage colony stimulating factor (Sigma-Aldrich, USA) – containing L929 supernatant for 6–9 days. Next, BMDMs were harvested with cold PBS (1X, 0.0067 M (PO_4^{3-}); Hyclone Laboratories, Inc., Logan, USA) and resuspended in medium without L929 supernatant for further study. As for the identification of BMDMs (Figure S23, Supporting Information), surface markers of BMDMs (i.e., CD11b and F4/80) were verified by flow cytometry and confocal laser scanning microscopy (CLSM; TCS SP8; Leica Microsystems Nussloch GmbH, Nussloch, Germany). To simulate the microenvironments of macrophages in a diabetic wound, BMDMs were further treated with high glucose (25 mM glucose) and 100 ng mL^{-1} LPS (Sigma-Aldrich, USA).

miR-4645-5p Gene Knockout: BMSCs were transfected with 50 nM of miR-4645-5p inhibitor to knock down miR-4645-5p gene, using Lipofectamine™ 2000 Transfection Reagent (11 668 019; ThermoFisher Scientific, Inc., Waltham, USA). An equal concentration of a nontargeting control (NC) sequence (50 nM) was applied as a control for non-sequence-specific effects in miRNA experiments. miR-4645-5p inhibitor and miR-NC were purchased from Guangzhou RiboBio Co., Ltd. (Guangzhou, China). The sequence of miR-4645-5p inhibitor was as follows: 5'-ACAAUAUUUCUUGCCUGGU-3'.

Exosome Isolation and Identification: Exosomes were extracted from hyBMSCs via using ultracentrifugation according to the previous study.[16b] Figure S1 (Supporting Information) shows the detailed procedures of exosome preparation and characterization. Prior to exosome isolation, BMSCs underwent pretreatment with 1% O_2 hypoxia at 37°C for 48 h using an oxygen control incubator (Smartor 118pro; Ningbo HUAYI Ningchuang Intelligent Technology Co., Ltd., China) that was filled with 5% CO_2 and 94% N_2. Nanosight LM10 System (Malvern Panalytical Ltd., Malvern, UK) and FE-TEM (Tecnai 12; Royal Philips, Amsterdam, Netherlands) were applied to observe the dimension and morphology of hyBMSC-Exos. The concentration of proteins in the exosomes was determined using Pierce™ Rapid Gold BCA Protein Assay Kit (ThermoFisher, USA).

Synthesis of Chi-GA Conjugates: EDC/NHS coupling reaction was utilized to synthesize Chi-GA conjugates.[22b] In brief, 0.99 g 4-morpholineethanesulfonic acid (MES; 99%; Macklin Biochemical Co., Ltd., Shanghai, China) was dissolved in 100 mL distilled water with a resistivity of 18.25 MΩ·cm. Then, 1.00 g (≈ 6.20 mmol in terms of repeating unit) Chi (low molecular weight; Sigma-Aldrich, USA) was added into the MES solution. Afterward, 1.21 g EDC·HCl (98%; Aladdin Biochemical Technology Co., Ltd., Shanghai, China), 0.73 g NHS (98%; Aladdin, China), and 0.53 g GA (99%; Macklin, China) were orderly dissolved in the Chi/MES solution. The mixture was vigorously agitated at room temperature for 24 h under the shielding of argon gas, and its pH value was maintained at 5.4-5.5 using either 1 M HCl or 1 M NaOH solution. Subsequently, the reaction solution was dialyzed in a dialysis bag (MWCO 3500 Da; Sangon Biotechnology Co., Ltd., Shanghai, China) against distilled water supplementing with 10 mM NaCl for a duration of 72 h.[22b] This was then followed by an additional dialysis against distilled water for 12 h. The dialysate was replaced with fresh medium every 6 h. The resulting solution was lyophilized to collect solid-state Chi-GA conjugates. The conjugates were a solid resembling cotton, with a greyish-green color. They were stored at a temperature of −20°C for future use. ^{1}H NMR spectra of liquid samples including Chi and Chi-GA (20 mg mL^{-1} in D_2O) were recorded using Bruker NMR spectrometer (Avance III HD 500 MHz; Bruker Co., Billerica, USA). FTIR spectra of Chi and Chi-GA powders were obtained using KBr disks on a Nicolet FTIR spectrometer (Summit iS50 with Everest ATR Accessory; Thermo, USA). Using a UV/VIS/NIR spectrophotometer (Lambda 1050+2D; PerkinElmer, Inc., Waltham, USA), the UV–vis absorption spectra of Chi and Chi-GA (2.5 mg mL^{-1}) were recorded in the range of 200 to 600 nm.

Synthesis of OHA: OHA was synthesized by $NaIO_4$ oxidation method.[34,35a] To create 50 mL solution of hyaluronic acid (HA) with a concentration of 2% (w/v), 1.00 g HA (800 KDa-1.0 MDa; Aladdin, China) was dissolved into 50 mL distilled water. Next, 0.50 grams $NaIO_4$ (≥ 99.5%; Macklin, China) were dissolved in another 50 milliliters of distilled water and then slowly introduced into the HA solution. The reaction was maintained in a dim setting at ambient temperature for a duration of 4 h. After that, 1 mL ethylene glycol (analytical reagent, 98%; Macklin, China) was added to terminate the oxidation reaction. Subsequently, the solution was dialyzed in a dialysis bag (MWCO 12 000 Da; Sangon, China) against distilled water at room temperature for 12 h. The dialysate was replaced with fresh medium every 6 h. The resulting solution was lyophilized to collect solid-state OHA. The final product was a solid resembling white cotton, which was kept at a temperature of minus 20 degrees Celsius for future utilization. ^{1}H NMR spectra of liquid samples including HA and OHA (20 mg mL^{-1} in D_2O) were recorded with Bruker NMR spectrometer. FTIR spectra of HA and OHA powders were obtained using Nicolet FTIR spectrometer.

Preparation of CG-OHA Hydrogel: First, Chi-GA conjugates were dissolved in PBS (pH = 7.4) to prepare 3% (w/v) Chi-GA solution. In the same way, a solution of OHA with a concentration of 4% (w/v) was acquired. A homogenous hydrogel without hyBMSC-Exos, i.e., CG-OHA hydrogel, was formed by mixing Chi-GA and OHA solution in a volume ratio of 10 : 1. The hydrogel should be newly prepared when it will be used.

Preparation of CG-OHA@Exo Hydrogel: A uniform solution was firstly prepared by combining 1 mL of 3% (w/v) Chi-GA with 225 µL of concentrated hyBMSC-Exos solution (5 mg mL^{-1}). Then, a homogenous hydrogel containing 100 µg mL^{-1} hyBMSC-Exos, i.e., CG-OHA@Exo hydrogel, was formed by adding 100 µL of 4% (w/v) OHA solution. The hydrogel should be newly prepared when it will be used.

Characterization of the Hydrogels: Surface morphology of two types of hydrogels was observed by FE-SEM (SU8100; Hitachi Ltd., Tokyo, Japan) equipped with EDS. XPS (Escalab 250Xi; ThermoFisher, USA) analysis was used to analyze the elemental composition of the hydrogels. A rotational rheometer (HAAKE MARS III; ThermoFisher, USA) was utilized to investigate rheological properties of the hydrogels. Immediately after gelation, the hydrogels were examined for their storage modulus (G') and loss modulus (G''). The experiments were conducted at a temperature of 25°C, utilizing a parallel plate (20 mm) with a plate gap of 1000 µm. Frequency sweeps were performed at oscillation frequencies ranging from 0.1 to 100 rad s^{-1} with a strain level of 1%. Strain sweeps were carried out using a fixed oscillation frequency of 10 rad s^{-1} and variable applied strain of 0.1-1000%. G' and G'' of the hydrogels during 3 cycles between 1% and 400% oscillation strain were measured with a fixed oscillation frequency of 10 rad s^{-1} to observe the self-healing property of the hydrogels.

Evaluation of Hydrogels' Injectability and Moldability: Initially, the effect of shear rate on hydrogels' viscosity was investigated by using a shear thinning test to evaluate their injectability. In order to visually observe the injectability of CG-OHA@Exo hydrogel, a certain volume of hydrogel was placed into a syringe and subsequently pushed out through the nipple. A

brief video was captured to document the procedure (Movie S1, Supporting Information). To assess the moldability of CG-OHA@Exo hydrogel, it was first applied to the index finger joint, followed by bending the joint and observing its macro-morphology at various angles and rates of flexion and extension. A brief video was captured to document the procedure (Movie S2, Supporting Information).

Evaluation of Hydrogels' Swelling Properties: The newly prepared hydrogels (1 mL) were freeze dried and then weighed immediately after they were taken out. Next, the dry hydrogels were immersed into 50 mL preheated PBS (pH = 7.4). They were then incubated at 37°C for a certain interval of time. The hydrogels were taken out and weighed after the removal of superfluous water with filter papers. The swelling ratios of the hydrogels were calculated as the following formula: $((W_s\text{-}W_d)/W_d) \times 100\%$, where W_d and W_s represent the weight of a hydrogel at the dry and swollen states, respectively. When the weight of the soaked hydrogels no longer increased gradually with time, it was considered that the swelling equilibrium state had been reached, and the swelling ratios at this time were defined as equilibrium swelling ratios (ESR).

Hemolysis Assay: The investigation of different hydrogels' hemolysis ratios was conducted on the basis of a study that was previously documented.[22b] The experiment involved the use of male New Zealand white rabbits, weighing between 2.0 and 2.5 kilograms, to obtain whole blood samples. The entire procedure involving animal utilization was conducted in accordance with the regulations set by the Institutional Animal Care and Use Committee of China and was authorized by the Animal Ethics Committee of Shenzhen People's Hospital (Approval number: AUP-220516-SY-0242-01). Following the collection of rabbit blood through centrifugation at a speed of 3500 revolutions per minute (equivalent to 1566 times the force of gravity) for a duration of 10 min, the red blood cells were subsequently rinsed three times with PBS. Subsequently, a solution of erythrocytes diluted with PBS was prepared by combining 5 milliliters of purified red blood cells with 95 milliliters of PBS. The hydrogel freeze-dried powder was dispersed into PBS to create a hydrogel dispersion liquid of a predetermined concentration. Following that, 500 microliters of dispersion liquid were mixed completely with 500 microliters of erythrocyte/PBS solution in a 2 mL centrifuge tube. The tube was placed in an incubator set at a temperature of 37 degrees Celsius for a duration of 60 minutes. Subsequently, it was subjected to centrifugation at a speed of 3500 revolutions per minute (equivalent to 1566 times the force of gravity) for a period of 10 minutes. Afterwards, the supernatant was assessed for absorbance at 540 nm using a Tecan Spark 10 M automatic microplate reader (Tecan Group Ltd., Männedorf, Switzerland). All the experiments were replicated 3 times for each sample. Hemolysis ratios of the hydrogels were calculated using the formula: $[(A_s - A_n)/(A_p - A_n)] \times 100\%$, where A_s, A_n, and A_p represent the absorbance values of the supernatant, negative (PBS), and positive (0.1% Triton X-100) groups, respectively.

Total Antioxidant Capacity Assay: Total antioxidant capacity of various hydrogels was investigated by using a FRAP method, making slight adjustments based on the previous research.[22b,c] To begin with, a hydrogel suspension with a predetermined concentration was prepared by dispersing the hydrogels' freeze-dried powders into PBS. Next, a combination of 50 µL hydrogel suspension and 500 µL FRAP working solution (Beyotime Biotechnology Co., Jiangsu, China) was placed in an incubator at a temperature of 37 degrees Celsius for a duration of 10 min. Immediately afterwards, the combination was subjected to centrifugation at a speed of 4500 revolutions per minute (equivalent to 3524 times the force of gravity) for a duration of 10 min, and 150 microliters of the resulting liquid above the sediments were moved into a cell-culture plate containing 96 wells. A microplate reader was employed to measure the absorbance of the supernatant at 593 nm. In the meantime, a calibration curve was created using $FeSO_4$. Total antioxidant capacity of various hydrogels was then calibrated with the standard curve and indicated as mM $FeSO_4$ (mg hydrogel)$^{-1}$. Total antioxidant capacity of CG-OHA hydrogel with various concentration was indicated as mM $FeSO_4$.

Intracellular ROS Scavenging Testing: Briefly, a total of 20 000 BMDMs were placed in a cell-culture plate containing 24 wells and cultured for a duration of 24 h. In the absence of light, the cells were exposed to 10 µM 2',7'-dichlorodihydrofluorescein diacetate (DCFH-DA; BioReagent, ≥ 95% (HPLC); Sigma-Aldrich, USA) (dissolved in serum-free medium) for a duration of 30 min. Whereafter, DCFH-DA was eliminated and the cells were subjected to incubation with PBS that contained H_2O_2 (100 µM) and the hydrogels (1 mg mL^{-1}) for another 30 min. After that, representative fluorescence images were obtained using an inverted fluorescence microscope (Zeiss Axio Observer Z1; Carl Zeiss, Inc., Germany). Relative ROS levels were analyzed by Image Pro Plus version 6.0 (IPP 6.0; Media Cybernetics, Inc., Rockville, USA).

Evaluation of In Vitro Antibacterial Properties: Different hydrogels were tested for their in vitro antibacterial capabilities using *S. aureus* (ATCC6538; Guangdong HuanKai Microbial Sci. & Tech. Co., Ltd., Guangzhou, China) and *E. coli* (ATCC25922; Huankai Microbial, China). On the one hand, to investigate the hydrogels' antibacterial efficiency, 1×10^6 bacteria were firstly dispersed into one milliliter of hydrogel suspension (1 mg mL^{-1}, the solvent was a sterile liquid bacterial medium). Following incubation at a temperature of 37 degrees Celsius for a duration of 24 h, the mixed solution was diluted by a factor of 100000. Subsequently, 100 microliters of the solution were taken out to spread on sterile agar plates. Afterward, the plates were placed in an incubator at a temperature of 37°C for a duration of 24 h. Representative photographs of the plates were captured and the number of bacterial colonies was counted with IPP 6.0. Antibacterial rate (%) was calculated as follows: $((N_{Control}\text{-}N_{Target\ group})/N_{Control}) \times 100\%$, where $N_{Control}$ and $N_{Target\ group}$ represent the number of colonies in the control and target groups. On the other hand, growth profiles of *E. coli* and *S. aureus* were examined when coexisting with suspensions of CG-OHA and CG-OHA@Exo hydrogels for a duration of 72 h. In brief, a mixture of 1 million bacteria and 1 milligram of freeze-dried hydrogel powders were dispersed into 1 milliliter liquid bacterial medium. Within 72 h of co-culture, the bacteria were collected by centrifugation at 2, 4, 6, 8, 10, 12, 24, 48 and 72 h, and re-suspended with equal volume PBS solution. A microplate reader was applied to measure the absorbance of the solution at a wavelength of 600 nm.

Cell Viability Assay: Cell viability of BMDMs and HaCaT cells was assessed using CellTiter 96® Aqueous One Solution Cell Proliferation Assay (Promega Co., Madison, USA) following a 24-hour treatment with the hydrogels in this research. In brief, BMDMs or HaCaT cells were introduced into a cell-culture plate containing 96 wells at an initial population of 5000 cells. They were then cultured until they achieved a 90% confluence. Afterwards, the medium was substituted with 1 milliliter new medium that contained the hydrogels at a concentration of 1 milligram per milliliter. After culturing for a predetermined time, cell medium was changed to 80 µL 3-(4,5-dimethylthiazol-2-yl)−5-(3-carboxymethoxyphenyl)−2-(4-sulfophenyl)−2H-tetrazolium, inner salt (MTS). Following this, the plate was placed in an incubator at a temperature of 37 degrees Celsius for an additional 4 h. Finally, an automatic microplate reader was employed to measure the absorbance of the solution at a wavelength of 490 nm.

Live/Dead Cell Staining: In cell-culture plates containing 24 wells, the cells (BMDMs and HaCaT cells) were initially seeded at a density of 1×10^4 cells cm^{-2}. Following a 24-hour incubation, the original medium was substituted with 1 milliliter of new medium containing the hydrogels at a concentration of 1 milligram per milliliter. After one day, the cells were rinsed three times with PBS, and 180 microliters of Calcein AM/PI working solution (Beyotime, China) were introduced. The cells were subsequently placed in a dark environment and incubated for an additional 30 minutes. Ultimately, an inverted fluorescence microscope was applied to capture representative fluorescence images.

In Vivo Degradation of Hydrogels: The entire procedure involving animal utilization was conducted in accordance with the regulations set by the Institutional Animal Care and Use Committee of China and was authorized by the Animal Ethics Committee of Shenzhen People's Hospital (Approval number: AUP-220516-SY-0242-01). Diabetic wound models were established by high fat feeding and streptozocin injection using 4-week-old male Swiss mice obtained from ENSIWEIER Biotechnology Co., Ltd. (Chongqing, China). The mice were only deemed fit for the experiment if their blood sugar levels were consistently higher than 11.1 mM throughout the experiment, otherwise they would be removed from the experiment and euthanized. The diameter of a full-thickness wound was 8 mm. After the wounds were covered with 100 µL hydrogels, the mice were kept

under normal conditions for four days. During this period, no more dosing was performed. At day 4 after surgery, representative wound photographs were recorded, and the residual hydrogels were carefully removed and weighed.

Stability and Release of Exosomes in CG-OHA@Exo Hydrogel: DiR (≥ 98%; Solarbio Science & Technology Co., Beijing, China) was used to label exosomes in order to monitor their release profile from CG-OHA@Exo hydrogel in real time. 1 milliliter of CG-OHA@Exo sample was submerged in 1 milliliter of PBS and incubated in a 37°C thermostatic incubator. At the indicated time points, the supernatant was replaced with 1 milliliter of new PBS and then analyzed by an IVIS (IVIS® Lumina S5; PerkinElmer, Inc.) to detect the release ratio of exosomes. Also, BCA protein assay was conducted to quantitatively determine the number of released exosomes from CG-OHA@Exo hydrogel. To further evaluate the retention of exosomes after administration in vivo, the biodistribution of DiR-labeled exosomes in diabetic wounds was monitored by an IVIS. The entire procedure involving animal utilization was conducted in accordance with the regulations set by the Institutional Animal Care and Use Committee of China and was authorized by the Animal Ethics Committee of Shenzhen People's Hospital (Approval number: AUP-220516-SY-0242-01). The excisional wounds (one spot per mouse) were made in the backs of the mice. DiR-labeled exosomes chemically immobilized in the hydrogel at a concentration of 100 μg mL^{-1} (CG-OHA@Exo) or suspended in PBS (Exo) were topically applied to each wound on day 0. At the indicated time points, mice were imaged immediately using an IVIS.

Exosome Uptake Assay: In order to assess the uptake efficiency of hyBMSC-Exos by BMDMs, the exosomes were firstly labeled using PKH67 Green Fluorescent Cell Linker Mini Kit (Sigma-Aldrich, USA). After that, PKH67-labeled exosomes chemically immobilized in the hydrogel at a concentration of 100 μg mL^{-1} (CG-OHA@Exo) or suspended in PBS (Exo) were co-cultured with BMDMs for 48 h. Subsequently, representative fluorescence images were captured by CLSM and the uptake efficiency of hyBMSC-Exos by BMDMs was evaluated via measuring the fluorescence intensity of the images.

Fluorescence In Situ Hybridization (FISH): A specific miR-4646-5p FISH probe labeded by 6-Carboxyfluorescein (99.88%; MedChemExpress LLC, New Jersey, USA) was designed and utilized in the following processes. BMDMs were cultured in a cell-culture plate containing 96 wells at an initial density of 5000 cells, and incubated for a duration of 24 h. Following this, the cells were treated with exosomes chemically immobilized in hydrogel at a concentration of 100 μg mL^{-1} (CG-OHA@Exo) or suspended in PBS (Exo). The cell slide was prepared and immobilized with 4% paraformaldehyde (analytical reagent, powder; Aladdin, China) and washed with PBS 3 times. After that, dilute probe solution was dripped onto the cell slide. Afterwards, in situ hybridization was performed in a humidified chamber at 42°C for 48 h. And miR-4645-5p signals were detected using FISH Kit (RiboBio Biotechnology Co., Ltd., Guangzhou, China) based on the manufacturer's instruction. Representative fluorescence images were captured using CLSM, and the fluorescence intensity of miR-4645-5p was measured by IPP 6.0.

Flow Cytometric Staining, Sorting, and Counting: To identify BMDMs isolated from mouse femurs and tibias, the cells were stained with anti-mouse/human CD11b (ab8878; Abcam PLC, Cambridge, England) (1 : 1000) and anti-mouse F4/80 (ab6640; Abcam, England) (1: 10) antibodies. To detect macrophage subsets in vitro, BMDMs were firstly treated with different hydrogels and then stained with anti-mouse/human/rat/chicken iNOS (bs-2072R; BIOSS Biotechnology Co., Ltd., Beijing, China) (1 : 100), anti-mouse/rat/human Arg1 (16001-1-AP; Proteintech Group, Inc., Rosemont, USA) (1 : 500), anti-mouse CD80 (ab106162; Abcam, England) (1 : 100), and anti-mouse/rat/human CD206 (18704-1-AP; Proteintech, USA) (1 : 200) antibodies. For the detection of macrophage subsets during wound healing, cells from the wound sites need to be prepared as single-cell suspensions, and then incubated with FITC anti-mouse CD16/CD32 (FITC-65080; Proteintech, USA) for 15 min on ice to prevent non-specific binding of subsequent antibodies. Subsequently, the cells were washed and stained with iNOS, Arg1, CD80, and CD206 antibodies. All the above labeled cells were further sorted on FongCyte™ 3 laser 14-color flow cytometer (Beijing Challen Biotechnology Co., Ltd., Beijing, China).

Immunofluorescence Staining: The described procedures for immunofluorescent staining involved permeabilizing the samples (i.e., immobilized hyMSCs, BMDMs, or tissue slides) with 0.3% Triton X-100 for 10 min, followed by blocking with 5% albumin from bovine serum (biotechnology grade, 96%; Aladdin, China) for 30 min. Afterwards, the samples were left to incubate with the primary antibodies overnight at a temperature of 4 degrees Celsius. The used primary antibodies were as follows: anti-human HIF-1α (ab1; Abcam, England) (1 : 200), iNOS (1 : 200), Arg1 (1 : 200), anti-rat/chicken/human SREBP2 (ab30682; Abcam, England) (1 : 1000), CD11b (1 : 50), anti-mouse/rat CD31 (ab222783; Abcam, England) (1 : 100), and anti-mouse/rat/human α-SMA (19 245; Cell Signaling Technology, Inc., Boston, USA) (1 : 400). After goat anti-rabbit IgG (Wuhan Boster Biological Technology Co., Ltd., Wuhan, China) (1 : 1000), DyLight 488-conjugated goat anti-rabbit IgG (Boster, China) (1: 1000), and Cy3-labeled goat anti-rabbit IgG (Boster, China) (1: 1000) were utilized at 37 degrees Celsius for a duration of 1 h, the nuclei of cells were stained with 4',6-diamidino-2-phenylindole (DAPI) dihydrochloride (BioReagent, ≥ 98% (HPLC and TLC); Sigma-Aldrich, USA) at 37°C for 10 min. Representative fluorescent images were obtained by CLSM. IPP 6.0 was used to analyze the relative coverage area of the target analytes.

RT-qPCR: AG RNAex Pro RNA Reagent (Accurate Biotechnology (Hunan) Co., Ltd., Changsha, Hunan) was utilized to extract total RNA from cells and exosomes. According to the provided protocol, the extracted RNAs were further reverse-transcribed using miRNA First Strand cDNA Synthesis (Tailing Reaction) Kit (Sangon, China). Next, a Real-Time PCR system (ABI StepOne Plus; Thermo Fisher, USA) was used to analyzed the above synthesized cDNA with the primers shown in Table S1 (Supporting Information). Amplification was performed by using the following PCR program: stage 1, activation at 50°C for 2 min; stage 2, pre-soak at 95°C for 10 min; stage 3, denaturation at 95°C for 15 sec and annealing at 60°C for 1 min; stage 4, melting curve at 95°C for 15 sec, 60°C for 15 sec and 95°C for 15 sec. The glyceraldehyde-3-phosphate dehydrogenase (GAPDH) was used for normalization and the relative expression levels were assessed using the comparative $2^{-\Delta\Delta Ct}$ method.

ELISA: Bone marrow-derived macrophages were seeded in a cell-culture plate with 96 wells at an initial density of 5000 cells, and allowed to grow until they reached 90% confluency. After the cells were treated under the indicated conditions, the medium was collected to determine the amount of IL-1β, IL-6, IL-12, IL-23, IL-10, IGF, TGF-β1, and VEGF according to the guidelines of the ELISA kits (R&D Systems, Inc., Minneapolis, USA). The concentration of the analytes was determined from a standard absorbance curve.

Western Blotting: There are typical processes as follows: The extracted proteins from exosomes, cells, and tissues loaded and run on a 6–10% SDS-containing polyacrylamide (SDS/PAGE) gel, and then transferred onto polyvinylidene fluoride (PVDF) membranes (IPVH00010; Merck Millipore, Berlin, Germany). Following a 1-hour blockage at room temperature using 5% nonfat milk, the membranes were incubated with primary antibodies overnight at 4 degrees Celsius. Subsequently, the PVDF membranes were exposed to secondary antibodies at room temperature for a duration of 1 h. Millipore's enhanced chemiluminescence system (Merck Millipore, Berlin, Germany) and MultiImage™ Light Cabinet (Version 5.5; Alpha Innotech Corp., San Leandro, USA) were utilized to visualize and detect the protein bands. And the intensity of each band was calculated and analyzed by ImageJ software. The following antibodies were used for western blotting: anti-human CD9 (ab263019; Abcam, England) (1 : 1000), anti-human CD63 (ab134045; Abcam, England) (1 : 10 000), anti-mouse/rat/human CD81 (ab109201; Abcam, England) (1 : 10 000), iNOS (1 : 300), Arg1 (1 : 20 000), SREBP2 (1 : 200), anti-mouse/rat/human laminin beta 1 (LAMB1; 13 435; Cell Signaling Technology, USA) (1 : 1000), anti-human MAPKAPK2 (ab32567; Abcam, England) (1 : 1000), anti-mouse/human TNF-α (ab215188; Abcam, England) (1 : 1000), and anti-mouse/rat/hamster/monkey/dog/human β-actin (3700; Cell Signaling Technology, USA) (1 : 1000).

Surgical Procedures of In Vivo Diabetic Wound Management: The entire procedure involving animal utilization was conducted in accordance with the regulations set by the Institutional Animal Care and Use Committee of China and was authorized by the Animal Ethics Committee of

Shenzhen People's Hospital (Approval number: AUP-220516-SY-0242-01). Diabetic wound models were established using 8-week-old male db/db diabetic mice purchased from Shanghai SLAC Labortory Animal Co., Ltd. (Shanghai, China). Following the administration of anesthesia, two round excisional wounds measuring 1 centimeter in diameter and penetrating through all layers of tissue were surgically made on the dorsal region of db/db mice. Then, 200 µL samples were topically applied to each wound on three consecutive days (days 0, 1 and 2). 200 µL PBS was utilized as a control. The wounds were covered with 3 M Tegaderm^{TM} films (3 M Deutschland GmbH, Neuss, Germany). Photographs were taken of the wound sites at day 0, 4, 8, 12, and 14 post-wounding. The measurement of wound areas and traces in each group were conducted using IPP 6.0 and Adobe Photoshop CS5 Extended version 12.0 (Ps CS5; Adobe Systems, Inc., USA), respectively. At day 6 and 10 after surgery, a portion of mice from each group were euthanized, and a biopsy punch with 15 mm diameter was employed to collect newly formed skin tissue. The collected tissue was promptly treated with 10% formaldehyde solution (analytical reagent, 37 wt.% in H_2O, containing 10–15% methanol stabilizer; Macklin, China) that had been chilled with ice, in preparation for future use.

Histological Analysis: Following the removal of moisture through a sequence of ethanol and xylene, the preserved skin tissue was subsequently encased in paraffin. Sections of wound sites, with 5 µm thickness, were sliced and treated with H&E dye solution to assess histological characteristics of recently developed skin tissue using a light microscope (Leica DM2000; Leica Inc., Germany). Additionally, Masson's trichrome staining was performed for observing the degree of collagen maturity. Also, immunofluorescent staining of iNOS, CD11b, Arg 1, CD31, and α-SMA was conducted according to the processes described in the section of 2.13. Representative optical and fluorescent images were obtained using light microscope and CLSM, respectively. IPP 6.0 was applied to analyze the relative coverage area of the target analytes, which was limited to the recently developed skin tissue.

Statistical Analysis: All experiments were performed at least in triplicate in order to be eligible for the indicated statistical analysis. GraphPad Prism 8.0 (GraphPad Software LLC, San Diego, USA) was used for statistical comparisons. To assess the normality of the data, Shapiro-Wilk test was utilized. If the data sets met the normality condition, the difference between the data was analyzed using an unpaired t-test; otherwise, Wilcoxon test was employed. For three or more groups, statistical significance was assessed using one-way analysis of variance (ANOVA). Two-way ANOVA was used to evaluate comparisons between two or more groups at various time points. Following the ANOVA, the Bonferroni method was employed to compare multiple groups. A difference was considered statistically significant if $p < 0.05$.

Supporting Information

Supporting Information is available from the Wiley Online Library or from the author.

Acknowledgements

This work was financially sponsored by the National Natural Science Foundation of China (Nos. 82002272 and 82060350), the China Postdoctoral Science Foundation (Nos. 2021M701434 and 2022M711335), the Industry-university-research Innovation Fund of Higher Education of China (No. 2021JH028), the Science and Technology Innovation Committee of Shenzhen (No. JCYJ20220530152015036), and the Guangdong Basic and Applied Basic Research Foundation (No. 2022A1515110490).

Conflict of Interest

The authors declare no conflict of interest.

Author Contributions

Y.S. and S.W. contributed equally to this work. Y.S. designed the study, performed in vitro and in vivo study, analyzed most of the data, wrote the original draft, and revised the paper. S.W. assisted in study design, carried out in vitro and in vivo study, assisted data analysis, wrote the original draft, and revised the paper. K.W. assisted in materials experiments and modified the paper. R.Y., D.L., H.L., and T.Q. assisted in study design and revised the paper. K.Q. and Y.H. assisted in rat experiments and modified the paper. H.W. supervised the project and revised the paper. K.X. designed the study, carried out the experimental work related with materials, assisted data analysis, wrote the original draft, modified the paper, and supervised the project.

Data Availability Statement

Research data are not shared.

Keywords

diabetic wound healing, exosomes, hydrogel, hypoxic mesenchymal stem cells, macrophage dysfunction

Received: October 13, 2023
Revised: December 18, 2023
Published online:

[1] C. K. Sen, *Adv. Wound Care* **2019**, *8*, 39.
[2] G. Theocharidis, B. E. Thomas, D. Sarkar, H. L. Mumme, W. J. R. Pilcher, B. Dwivedi, T. Sandoval-Schaefer, R. F. Sîrbulescu, A. Kafanas, I. Mezghani, P. Wang, A. Lobao, I. S. Vlachos, B. Dash, H. C. Hsia, V. Horsley, S. S. Bhasin, A. Veves, M. Bhasin, *Nat. Commun.* **2022**, *13*, 181.
[3] a) K. Ogurtsova, J. D. da Rocha Fernandes, Y. Huang, U. Linnenkamp, L. Guariguata, N. H. Cho, D. Cavan, J. E. Shaw, L. E. Makaroff, *Diabetes Res. Clin. Pract.* **2017**, *128*, 40; b) Y. Zhu, Z. Cankova, M. Iwanaszko, S. Lichtor, M. Mrksich, G. A. Ameer, *Proc. Natl. Acad. Sci. USA* **2018**, *115*, 6816; c) D. G. Armstrong, M. A. Swerdlow, A. A. Armstrong, M. S. Conte, W. V. Padula, S. A. Bus, *J. Foot Ankle Res.* **2020**, *13*, 16.
[4] a) A. J. Martí-Carvajal, C. Gluud, S. Nicola, D. Simancas-Racines, L. Reveiz, P. Oliva, J. Cedeño-Taborda, *Cochrane Database Syst. Rev.* **2015**, *10*, CD008548; b) Y. Du, M. Yu, J. Ge, P. X. Ma, X. Chen, B. Lei, *Adv. Funct. Mater.* **2015**, *25*, 5016; c) J. Boateng, O. Catanzano, *J. Pharm. Sci.* **2015**, *104*, 3653.
[5] A. Sindrilaru, T. Peters, S. Wieschalka, C. Baican, A. Baican, H. Peter, A. Hainzl, S. Schatz, Y. Qi, A. Schlecht, J. M. Weiss, M. Wlaschek, C. Sunderkötter, K. Scharffetter-Kochanek, *J. Clin. Invest.* **2011**, *121*, 985.
[6] K. A. Gallagher, A. Joshi, W. F. Carson, M. Schaller, R. Allen, S. Mukerjee, N. Kittan, E. L. Feldman, P. K. Henke, C. Hogaboam, C. F. Burant, S. L. Kunkel, *Diabetes* **2015**, *64*, 1420.
[7] a) R. Mirza, L. A. DiPietro, T. J. Koh, *Am. J. Pathol.* **2009**, *175*, 2454; b) T. Lucas, A. Waisman, R. Ranjan, J. Roes, T. Krieg, W. Muller, A. Roers, S. A. Eming, *J. Immunol.* **2010**, *184*, 3964; c) C. J. Ferrante, S. J. Leibovich, *Adv. Wound Care* **2012**, *1*, 10.
[8] L. Yan, K. Han, B. Pang, H. Jin, X. Zhao, X. Xu, C. Jiang, N. Cui, T. Lu, J. Shi, *Chem. Eng. J.* **2021**, *414*, 128836.
[9] a) S. W. Kim, G. B. Im, G. J. Jeong, S. Baik, J. Hyun, Y. J. Kim, C. Pang, Y. C. Jang, S. H. Bhang, *Biomaterials* **2021**, *275*, 120954; b) Y. Yuan, D. Fan, S. Shen, X. Ma, *Chem. Eng. J.* **2022**, *433*, 133859.
[10] a) A. Liu, D. Lin, H. Zhao, L. Chen, B. Cai, K. Lin, S. G. F. Shen, *Biomaterials* **2021**, *272*, 120718; b) W. Gao, J. Deng, J. Ren, W. Zhang,

Z. Wang, R. He, K. Wang, X. Shi, T. Liang, *Compos. Part B-Eng.* **2022**, *247*, 110315; c) E. J. Im, C. H. Lee, P. G. Moon, G. G. Rangaswamy, B. Lee, J. M. Lee, J. C. Lee, J. G. Jee, J. S. Bae, T. K. Kwon, K. W. Kang, M. S. Jeong, J. E. Lee, H. S. Jung, H. J. Ro, S. Jun, W. Kang, S. Y. Seo, Y. E. Cho, B. J. Song, M. C. Baek, *Nat. Commun.* **2019**, *10*, 1387.

[11] a) R. C. Lai, R. W. Y. Yeo, S. K. Lim, *Semin. Cell. Dev. Biol.* **2015**, *40*, 82; b) Y. Liu, Z. Zhang, B. Wang, Y. Dong, C. Zhao, Y. Zhao, L. Zhang, X. Liu, J. Guo, Y. Chen, J. Zhou, T. Yang, Y. Wang, H. Liu, S. Wang, *Small* **2022**, *18*, 2107354; c) J. Gan, L. Sun, G. Chen, W. Ma, Y. Zhao, L. Sun, *Adv. Healthcare Mater.* **2022**, *11*, 2201105.

[12] W. Ren, J. Hou, C. Yang, H. Wang, S. Wu, Y. Wu, X. Zhao, C. Lu, *J. Exp. Clin. Canc. Res.* **2019**, *38*, 62.

[13] M. Cao, Y. Zhao, T. Chen, Z. Zhao, B. Zhang, C. Yuan, X. Wang, L. Chen, N. Wang, C. Li, X. Zhou, *Biomaterials* **2022**, *288*, 121739.

[14] P. Eliasson, J. I. Jonsson, *J. Cell Physiol.* **2010**, *222*, 17.

[15] W. L. Grayson, F. Zhao, B. Bunnell, T. Ma, *Biochem. Biophys. Resh. Commun.* **2007**, *358*, 948.

[16] a) Y. Shi, S. Wang, W. Zhang, Y. Zhu, Z. Fan, Y. Huang, F. Li, R. Yang, *Stem Cell Res. Ther.* **2022**, *13*, 314; b) Y. Shi, S. Wang, D. Liu, Z. Wang, Y. Zhu, J. Li, K. Xu, F. Li, H. Wen, R. Yang, *Burns Trauma* **2024**, *12*, tkad058.

[17] J. Deng, X. Wang, W. Zhang, L. Sun, X. Han, X. Tong, L. Yu, J. Ding, L. Yu, Y. Liu, *Adv. Funct. Mater.* **2023**, *33*, 2211664.

[18] X. Liu, Y. Yang, Y. Li, X. Niu, B. Zhao, Y. Wang, C. Bao, Z. Xie, Q. Lin, L. Zhu, *Nanoscale* **2017**, *9*, 4430.

[19] a) X. Zhang, B. Sai, F. Wang, L. Wang, Y. Wang, L. Zheng, G. Li, J. Tang, J. Xiang, *Mol. Cancer* **2019**, *18*, 40; b) C. Zhang, K. Shao, C. Liu, C. Li, B. Yu, *Eur. Rev. Med. Pharmaco.* **2019**, *23*, 6691; c) J. Zhu, K. Lu, N. Zhang, Y. Zhao, Q. Ma, J. Shen, Y. Lin, P. Xiang, Y. Tang, X. Hu, J. Chen, W. Zhu, K. A. Webster, J. Wang, H. Yu, *Artif. Cell. Nanomed. B.* **2018**, *46*, 1659.

[20] a) D. Al Sulaiman, N. Juthani, P. S. Doyle, *Adv. Healthcare Mater.* **2022**, *11*, 2102332; b) P. Liu, Y. Xiong, L. Chen, C. Lin, Y. Yang, Z. Lin, Y. Yu, B. Mi, G. Liu, X. Xiao, *Chem. Eng. J.* **2022**, *431*, 132413; c) Q. Tang, B. Lu, J. He, X. Chen, Q. Fu, H. Han, C. Luo, H. Yin, Z. Qin, D. Lyu, L. Zhang, M. Zhou, K. Yao, *Biomaterials* **2022**, *280*, 121320.

[21] H. Shi, K. Pan, M. Dai, W. Wei, X. Liu, X. Li, *ACS Appl. Bio Mater.* **2022**, *5*, 4244.

[22] a) K. Xu, M. Zhou, M. Li, W. Chen, Y. Zhu, K. Cai, *Appl. Surf. Sci.* **2020**, *511*, 145569; b) K. Xu, S. Deng, Y. Zhu, W. Yang, W. Chen, L. Huang, C. Zhang, M. Li, L. Ao, Y. Jiang, X. Wang, Q. Zhang, *Adv. Healthcare Mater.* **2023**, *12*, 2301370; c) K. Xu, C. Mu, C. Zhang, S. Deng, S. Lin, L. Zheng, W. Chen, Q. Zhang, *Biomaterials* **2023**, *301*, 122268.

[23] S. Jin, Y. Wang, X. Wu, Z. Li, L. Zhu, Y. Niu, Y. Zhou, Y. Liu, *Adv. Mater.* **2023**, *35*, 2211602.

[24] K. A. Zarember, H. L. Malech, *J. Clin. Invest.* **2005**, *115*, 1702.

[25] R. J. Lobb, M. Becker, S. W. Wen, C. S. Wong, A. P. Wiegmans, A. Leimgruber, A. Möller, *J. Extracell. Vesicles* **2015**, *4*, 27031.

[26] K. W. Witwer, E. I. Buzás, L. T. Bemis, A. Bora, C. Lässer, J. Lötvall, E. N. Nolte-'t Hoen, M. G. Piper, S. Sivaraman, J. Skog, C. Théry, M. H. Wauben, F. Hochberg, *J. Extracell. Vesicles* **2013**, *2*, 20360.

[27] D. M. Pegtel, S. J. Gould, *Annu. Rev. Biochem.* **2019**, *88*, 487.

[28] a) D. K. Kim, S. Lee, M. Kim, Y. Jeong, S. Lee, *Chem. Eng. J.* **2021**, *406*, 127080; b) X. Xu, Y. Liang, X. Li, K. Ouyang, M. Wang, T. Cao, W. Li, J. Liu, J. Xiong, B. Li, J. Xia, D. Wang, L. Duan, *Biomaterials* **2021**, *269*, 120539.

[29] a) P. Huang, J. Bi, G. R. Owen, W. Chen, A. Rokka, L. Koivisto, J. Heino, L. Häkkinen, H. Larjava, *J. Invest. Dermatol.* **2015**, *135*, 3051; b) C. Charoenviriyakul, Y. Takahashi, M. Morishita, A. Matsumoto, M. Nishikawa, Y. Takakura, *Eur. J. Pharm. Sci.* **2017**, *96*, 316.

[30] a) L. Guo, T. Qiang, Y. Ma, L. Ren, C. Zhu, *ACS Sustainable Chem. Eng.* **2021**, *9*, 8393; b) Y. Zhao, L. Yang, M. Xu, H. Wang, X. Gao, B. Niu, W. Li, *Int. J. Biol. Macromol.* **2022**, *222*, 2987.

[31] K. Guzmán, B. Kumar, M. J. Vallejo, M. Grijalva, A. Debut, L. Cumbal, *Prog. Org. Coat.* **2019**, *129*, 229.

[32] X. Wang, Z. Jiang, J. Shi, C. Zhang, W. Zhang, H. Wu, *Ind. Eng. Chem. Res.* **2013**, *52*, 14828.

[33] R. Bai, H. Yong, X. Zhang, J. Liu, J. Liu, *Int. J. Biol. Macromol.* **2020**, *143*, 49.

[34] S. Wang, J. Chi, Z. Jiang, H. Hu, C. Yang, W. Liu, B. Han, *Carbohyd. Polym.* **2021**, *256*, 117519.

[35] a) W.-Y. Su, Y.-C. Chen, F.-H. Lin, *Acta Biomater.* **2010**, *6*, 3044; b) C. G. França, D. P. Sacomani, D. G. Villalva, V. F. Nascimento, J. L. Dávila, M. H. A. Santana, *Eur. Polym. J.* **2019**, *121*, 109288.

[36] Q. Li, S. Zhang, R. Du, Y. Yang, Y. Liu, Z. Wan, X. Yang, *ACS Appl. Mater. Interfaces* **2023**, *15*, 17562.

[37] T. H. Dai, M. Tanaka, Y. Y. Huang, M. R. Hamblin, *Expert Rev. Anti. – Infe.* **2011**, *9*, 857.

[38] Z. Ren, T. Ke, Q. Ling, L. Zhao, H. Gu, *Carbohyd. Polym.* **2021**, *273*, 118533.

[39] D.-S. Lee, J. Y. Je, *J. Agric. Food Chem.* **2013**, *61*, 6574.

[40] S. Shen, D. Fan, Y. Yuan, X. Ma, J. Zhao, J. Yang, *Chem. Eng. J.* **2021**, *426*, 130610.

[41] a) M. Schafer, S. Werner, *Pharmacol. Res.* **2008**, *58*, 165; b) B. Ponugoti, F. Xu, C. Zhang, C. Tian, S. Pacios, D. T. Graves, *J. Cell. Biol.* **2013**, *203*, 327.

[42] Y. Shi, S. Wang, R. Yang, Z. Wang, W. Zhang, H. Liu, Y. Huang, *Oxid. Med. Cell. Longev.* **2022**, *2022*, 1084006.

[43] a) F. N. Faruqu, J. T. Wang, L. Xu, L. McNickle, E. M. Chong, A. Walters, M. Gurney, A. Clayton, L. A. Smyth, R. Hider, J. Sosabowski, K. T. Al-Jamal, *Theranostics* **2019**, *9*, 1666; b) H. Choi, Y. Kim, A. Mirzaaghasi, J. Heo, Y. N. Kim, J. H. Shin, S. Kim, N. H. Kim, E. S. Cho, J. I.n Yook, T. H. Yoo, E. Song, P. Kim, E. C. Shin, K. Chung, K. Choi, C. Choi, *Sci. Adv.* **2020**, *6*, eaaz6980.

[44] a) H. Henriques-Antunes, R. M. S. Cardoso, A. Zonari, J. Correia, E. C. Leal, A. Jiménez-Balsa, M. M. Lino, A. Barradas, I. Kostic, C. Gomes, J. M. Karp, E. Carvalho, L. Ferreira, *ACS Nano* **2019**, *13*, 8694; b) P. Wang, G. Theocharidis, I. S. Vlachos, K. Kounas, A. Lobao, B. Shu, B. Wu, J. Xie, Z. Hu, S. Qi, B. Tang, J. Zhu, A. Veves, *J. Invest. Dermatol.* **2022**, *142*, 2508.

[45] C. He, S. Zheng, Y. Luo, B. Wang, *Theranostics* **2018**, *8*, 237.

[46] L. A. Mulcahy, R. C. Pink, D. R. Carter, *J. Extracell. Vesicles* **2014**, *3*, 24641.

[47] C. Lässer, *Biol. Ther.* **2015**, *15*, 103.

[48] a) E. Segura, C. Nicco, B. Lombard, P. Véron, G. Raposo, F. Batteux, S. Amigorena, C. Théry, *Blood* **2005**, *106*, 216; b) B. Yu, H. W. Kim, M. Gong, J. Wang, R. W. Millard, Y. Wang, M. Ashraf, M. Xu, *Int. J. Cardiol.* **2015**, *182*, 349.

[49] a) S. El-Andaloussi, Y. Lee, S. Lakhal-Littleton, J. Li, Y. Seow, C. Gardiner, L. Alvarez-Erviti, I. L. Sargent, M. J. Wood, *Nat. Protoc.* **2012**, *7*, 2112; b) A. Hoshino, B. Costa-Silva, T. L. Shen, G. Rodrigues, A. Hashimoto, M. T. Mark, H. Molina, S. Kohsaka, A. Di Giannatale, S. Ceder, S. Singh, C. Williams, N. Soplop, K. Uryu, L. Pharmer, T. King, L. Bojmar, A. E. Davies, Y. Ararso, T. Zhang, H. Zhang, J. Hernandez, J. M. Weiss, V. D. Dumont-Cole, K. Kramer, L. H. Wexler, A. Narendran, G. K. Schwartz, J. H. Healey, P. Sandstrom, et al., *Nature* **2015**, *527*, 329.

[50] R. Bhome, F. Del Vecchio, G. H. Lee, M. D. Bullock, J. N. Primrose, A. E. Sayan, A. H. Mirnezami, *Cancer Lett* **2018**, *420*, 228.

[51] C. Liu, C. Su, *Theranostics* **2019**, *9*, 1015.

[52] C. Wang, Q. Wang, W. Gao, Z. Zhang, Y. Lou, H. Jin, X. Chen, B. Lei, H. Xu, C. Mao, *Acta. Biomater.* **2018**, *69*, 156.

[53] S. Patel, S. Srivastava, M. R. Singh, D. Singh, *Biomed. Pharmacother.* **2019**, *112*, 108615.

[54] T. Yu, M. Gao, P. Yang, D. Liu, D. Wang, F. Song, X. Zhang, Y. Liu, *J. Cell. Physiol.* **2019**, *234*, 4217.

[55] A. Hassanshahi, M. Moradzad, S. Ghalamkari, M. Fadaei, A. J. Cowin, M. Hassanshahi, *Cells* **2022**, *11*, 2953.
[56] U. A. Okonkwo, L. A. DiPietro, *Int. J. Mol. Sci.* **2017**, *18*, 1419.
[57] a) M. T. Holderfield, C. C. W. Hughes, *Circ. Res.* **2008**, *102*, 637; b) G. Ferrari, B. D. Cook, V. Terushkin, G. Pintucci, P. Mignatti, *J. Cell. Physiol.* **2009**, *219*, 449.
[58] C. Tong, X. Zhong, Y. Yang, X. Liu, G. Zhong, C. Xiao, B. Liu, W. Wang, X. Yang, *Biomaterials* **2020**, *243*, 119936.
[59] A. Kusnadi, S. H. Park, R. Yuan, T. Pannellini, E. Giannopoulou, D. Oliver, T. Lu, K. H. Park-Min, L. B. Ivashkiv, *Immunity* **2019**, *51*, 241.
[60] M. S. Brown, J. L. Goldstein, *Cell* **1997**, *89*, 331.
[61] a) D. Brenner, H. Blaser, T. W. Mak, *Nat. Rev. Immunol.* **2015**, *15*, 362; b) G. D. Kalliolias, L. B. Ivashkiv, *Nat. Rev. Rheumatol.* **2016**, *12*, 49.
[62] M. B. Menon, M. Gaestel, *Trends Biochem. Sci.* **2018**, *43*, 170.
[63] L. Liu, K. Zhang, H. Sandoval, S. Yamamoto, M. Jaiswal, E. Sanz, Z. Li, J. Hui, B. H. Graham, A. Quintana, H. J. Bellen, *Cell* **2015**, *160*, 177.